Uromodulin regulates renal magnesium homeostasis through the ion channel transient receptor potential melastatin 6 (TRPM6)

Received for publication, June 8, 2018, and in revised form, August 21, 2018 Published, Papers in Press, August 23, 2018, DOI 10.1074/jbc.RA118.003950

Mingzhu Nie[‡1], Manjot S. Bal[‡1], Jie Liu[‡], Zhufeng Yang[§], Carolina Rivera[‡], Xue-Ru Wu[¶], Joost G. J. Hoenderop[‖], René J. M. Bindels[‖], Denise K. Marciano[§], and Matthias T. F. Wolf[‡2]

From the Departments of [‡]Pediatrics and [§]Internal Medicine, University of Texas Southwestern Medical Center, Dallas, Texas 75390, the [¶]Departments of Urology and Pathology, New York University School of Medicine, New York, New York 10016, and the [‖]Department of Physiology, Radboud Center for Molecular Life Sciences, Radboud University Medical Centre, 6525 GA Nijmegen, The Netherlands

Edited by Mike Shipston

Up to 15% of the population have mild to moderate chronic hypomagnesemia, which is associated with type 2 diabetes mellitus, hypertension, metabolic syndrome, and chronic kidney disease. The kidney is the key organ for magnesium homeostasis, but our understanding of renal magnesium regulation is very limited. Uromodulin (UMOD) is the most abundant urinary protein in humans, and here we report that UMOD has a role in renal magnesium homeostasis. *Umod*-knockout (*Umod*$^{-/-}$) mice excreted more urinary magnesium than WT mice and displayed up-regulation of genes promoting magnesium absorption. The majority of magnesium is absorbed in the thick ascending limb. However, both mouse strains responded similarly to the diuretic agent furosemide, indicating appropriate function of the thick ascending limb in the *Umod*$^{-/-}$ mice. Magnesium absorption is fine-tuned in the distal convoluted tubule (DCT) via the apical magnesium channel transient receptor potential melastatin 6 (TRPM6). We observed decreased apical Trpm6 staining in the DCT of *Umod*$^{-/-}$ mice. Applying biotinylation assays and whole-cell patch-clamp recordings, we found that UMOD enhances TRPM6 cell-surface abundance and current density from the extracellular space. UMOD physically interacted with TRPM6 and thereby impaired dynamin-dependent TRPM6 endocytosis. WT mice fed a low-magnesium diet had an increased urinary UMOD secretion compared with the same mice on a regular diet. Our results suggest that increased urinary UMOD secretion in low-magnesium states reduces TRPM6 endocytosis and thereby up-regulates TRPM6 cell-surface abundance to defend against further urinary magnesium losses.

This work was supported, in whole or in part, by National Institutes of Health Grants K08DK095994-04 (to M. T. F. W.), R03DK111776-01 (to M. T. F. W.), P30DK079328 (to M. T. F. W. and D. K. M.), and R01DK009478 (to D. K. M.) and the Children's Health System, Dallas (to M. T. F. W.). The authors declare that they have no conflicts of interest with the contents of this article. The content is solely the responsibility of the authors and does not necessarily represent the official views of the National Institutes of Health.
This article contains Table S1 and Fig. S1.

[1] Both authors contributed equally to this work.
[2] To whom correspondence should be addressed: Dept. of Pediatrics, University of Texas Southwestern Medical Center, 5323 Harry Hines Blvd., Dallas, TX 75390-9063. Tel.: 214-648-3438; Fax: 214-648-2034; E-mail: matthias.wolf@utsouthwestern.edu.

Mg^{2+} is often called the "forgotten" cation, although hypomagnesemia affects 15% of the general population (1). Overall, the impact of Mg^{2+} disturbances on public health is underappreciated (2–4). Mild to moderate hypomagnesemia does not cause acute symptoms and remains mostly undiagnosed and untreated (3). However, chronic hypomagnesemia has been associated with the development of common metabolic disorders, such as type 2 diabetes mellitus, hypertension, coronary artery disease, metabolic syndrome, nephrolithiasis, and chronic kidney disease (CKD)[3] (2–21). Hypomagnesemia also is a significant risk for cardiovascular disease and death (22–25). The major organ for regulated Mg^{2+} homeostasis is the kidney. About 10–25% of the filtered Mg^{2+} is absorbed in the proximal tubule and 50–70% in the thick ascending limb (TAL) of Henle. In the TAL, the positive lumen potential, generated by the Na^+-K^+-Cl^- cotransporter (NKCC2) and the renal outer medullary K^+ channel (ROMK), contribute to the paracellular absorption of Mg^{2+} (26). The final urinary Mg^{2+} concentration is determined by an active, transcellular, and regulated transport via the apical epithelial magnesium channel transient receptor potential melastatin 6 (TRPM6) in the distal convoluted tubule (DCT) (27, 28). Recessive mutations in *TRPM6* result in severe hypomagnesemia (29, 30). *Trpm6*$^{-/-}$ mice are embryonic lethal (31).

The regulation of renal Mg^{2+} homeostasis and TRPM6 remains largely unknown. The majority of TRPM6 channel regulation occurs either by (i) receptor-dependent pathways via insulin, epidermal growth factor (EGF), and receptor for activated protein C kinase 1 (RACK1) altering TRPM6 phosphorylation or (ii) increased channel mRNA expression by estrogen (32–37). Recently, the ADP-ribosylation factor–like GTPase 15 (ARL15) was also shown to influence Mg^{2+} absorption via TRPM6 and to modify glucose and lipid metabolism (38). A new mechanism for renal Mg^{2+} regulation was implied when mice fed a low-Mg^{2+} diet displayed increased renal Uromodu-

[3] The abbreviations used are: CKD, chronic kidney disease; DCT, distal convoluted tubule; DN, dominant-negative; EGF, epidermal growth factor; GPI, glycosylphosphatidylinositol; HA, hemagglutinin; HEK293 cells, human embryonic kidney cells; TAL, thick ascending limb; ZP, zona pellucida; HEDTA, *N*-(2-hydroxyethyl)ethylenediaminetriacetic acid; pF, picofarads; PV, parvalbumin.

lin (*Umod*) gene expression (39). This suggested a role for UMOD as part of a physiological response to hypomagnesemia (39). In fact, two different mutant *Umod* mouse models display urinary Mg^{2+} wasting (40, 41). UMOD is the most abundant protein in human urine; it protects against urinary tract infections and renal calcium crystal formation and is a promoter for hypertension (42–44). In this study, we wanted to analyze the role for UMOD in Mg^{2+} regulation and investigate the mechanism by which UMOD enhances TRPM6 cell-surface abundance from the extracellular space.

Results

Umod$^{-/-}$ mice display urinary Mg^{2+} wasting and decreased apical Trpm6 abundance in the DCT

Because up-regulation of UMOD mRNA in hypomagnesic mice suggested a role for UMOD in Mg^{2+} regulation, we studied whether *Umod*$^{-/-}$ mice excreted more urinary Mg^{2+} than WT animals. *Umod*$^{-/-}$ mice had almost twice the urinary Mg^{2+} compared with WT mice when fed a regular diet (Fig. 1*A*). Whereas there was no significant difference in serum Mg^{2+} between WT and *Umod*$^{-/-}$ mice at baseline (Fig. 1*B*), *Umod*$^{-/-}$ mice displayed up-regulated mRNA expression of *Trpm6*, *Hnf1b* (hepatocyte nuclear factor 1b), *Egf*, *Fxyd2b* (Na^+-K^+-ATPase regulatory protein), and parvalbumin (PV), all of which promote renal Mg^{2+} absorption (Fig. 1*C*), which is consistent with a Mg^{2+}-deficient state. It has been proposed that *Umod*$^{-/-}$ mice have a dysfunctional TAL, as they have a blunted response to furosemide (45, 46). As the majority of Mg^{2+} is absorbed in the TAL, we tested the TAL of WT and *Umod*$^{-/-}$ mice for the response to furosemide. At baseline, we detected in 9-month-old *Umod*$^{-/-}$ mice significantly higher urinary calcium (Ca^{2+}) and Mg^{2+} excretion (Table 1). However, we found no significant difference between WT and *Umod*$^{-/-}$ mice in response to furosemide administration regarding urine volume, sodium (Na^+), potassium (K^+), Ca^{2+}, or Mg^{2+} excretion (Table 1). We also detected appropriate response of the TAL to furosemide in 5-month-old *Umod*$^{-/-}$ mice (Table S1). As the TAL in *Umod*$^{-/-}$ mice responded well to furosemide, we wondered about other mechanisms for how UMOD could affect renal Mg^{2+} regulation. Therefore, we tested whether a lack of apical Trpm6 localization in the DCT contributes to renal Mg^{2+} wasting in *Umod*$^{-/-}$ mice. In WT and *Umod*$^{-/-}$ mice, immunofluorescent staining for the Na^+-Cl^- cotransporter (Ncc) and calbindin-D28K confirmed correct identification of the DCT (*b* and *c* in Fig. 1*D*). Ncc and calbindin-D28K expression appear similar in WT and *Umod*$^{-/-}$ animals (*b* and *c versus e* and *f* in Fig. 1*D*). However, evaluation of Trpm6 staining in the Ncc– and calbindin-D28K–positive tubules revealed less apical Trpm6 abundance in *Umod*$^{-/-}$ compared with WT mice (*a versus d* in Fig. 1*D*), despite an increase in *Trpm6* transcript in *Umod*$^{-/-}$ animals (Fig. 1*C*). Our data point to the DCT as the responsible nephron segment for urinary Mg^{2+} wasting in *Umod*$^{-/-}$ mice and suggest a post-transcriptional mechanism for UMOD regulation of TRPM6.

UMOD increases TRPM6 current density and TRPM6 cell-surface abundance

First, we determined in HEK293 cells whether UMOD increases TRPM6 mRNA or protein expression. Relative TRPM6 mRNA and protein expression was not enhanced in cells co-transfected with TRPM6 and UMOD compared with control (Fig. 2, *A* and *B*). UMOD did not increase total TRPM6 protein abundance at 24, 48, or 72 h (Fig. S1). To study whether UMOD has an effect on TRPM6 channel current density, we co-transfected HEK293 cells with TRPM6 and control or UMOD. Co-expression of TRPM6 and UMOD increased TRPM6 current density significantly by a factor of 4.6 compared with control (Fig. 2, *C* and *D*). For the subsequent experiments, UMOD enhanced TRPM6 current density in the range of 1.9–4.7-fold compared with control. This variability is most likely due to different transfection efficiency with each experiment. To test whether UMOD enhances TRPM6 cell-surface abundance, we performed biotinylation assays. TRPM6 cell-surface abundance was about 2.7-fold higher in cells co-transfected with UMOD compared with control plasmid (Fig. 2*E*). The increase of TRPM6 cell-surface abundance with UMOD was reasonably close to the observed increases in TRPM6 current density recorded for this work. Our data indicate that UMOD increases TRPM6 current density by enhancing the number of channels in the plasma membrane.

Extracellular UMOD increases TRPM6 current density in a dose-dependent fashion

The majority of UMOD is synthesized in the TAL, whereas TRPM6 is mostly localized in the more distal segment of the DCT (47–50). Proteolytic cleavage between the UMOD zona pellucida domain and the glycosylphosphatidylinositol (GPI) anchor releases UMOD into the ultrafiltrate (51). Therefore, we tested the hypothesis that UMOD enhances TRPM6 from the extracellular space. HEK293 cells were transfected either with control, WT UMOD, or C150S mutant UMOD (a known human mutation that results in UMOD retention in the endoplasmic reticulum and decreased UMOD secretion as previously shown by us) (52, 53). UMOD- and control-containing supernatant was harvested after 48 h and transferred onto TRPM6-expressing cells as described previously (52). After incubation overnight, WT UMOD–containing supernatant increased TRPM6 current density significantly compared with control– or C150S UMOD–containing supernatant (Fig. 3*A*). We confirmed an extracellular mechanism for up-regulation of TRPM6 current density by UMOD by performing a dose-response curve applying increasing dosages of purified UMOD. The half-maximal concentration for UMOD-mediated TRPM6 up-regulation was ~1 μg/ml (Fig. 3*B*). This value is estimated to be 10-fold lower than estimates of human urinary UMOD concentration and therefore is within physiological concentration ranges for UMOD (54, 55). Moreover, the addition of anti-UMOD antibody to TRPM6-transfected HEK293 cells incubated with UMOD-containing supernatant abrogated UMOD-mediated TRPM6 up-regulation (Fig. 3*C*). Collectively, these results strongly support a model by which UMOD

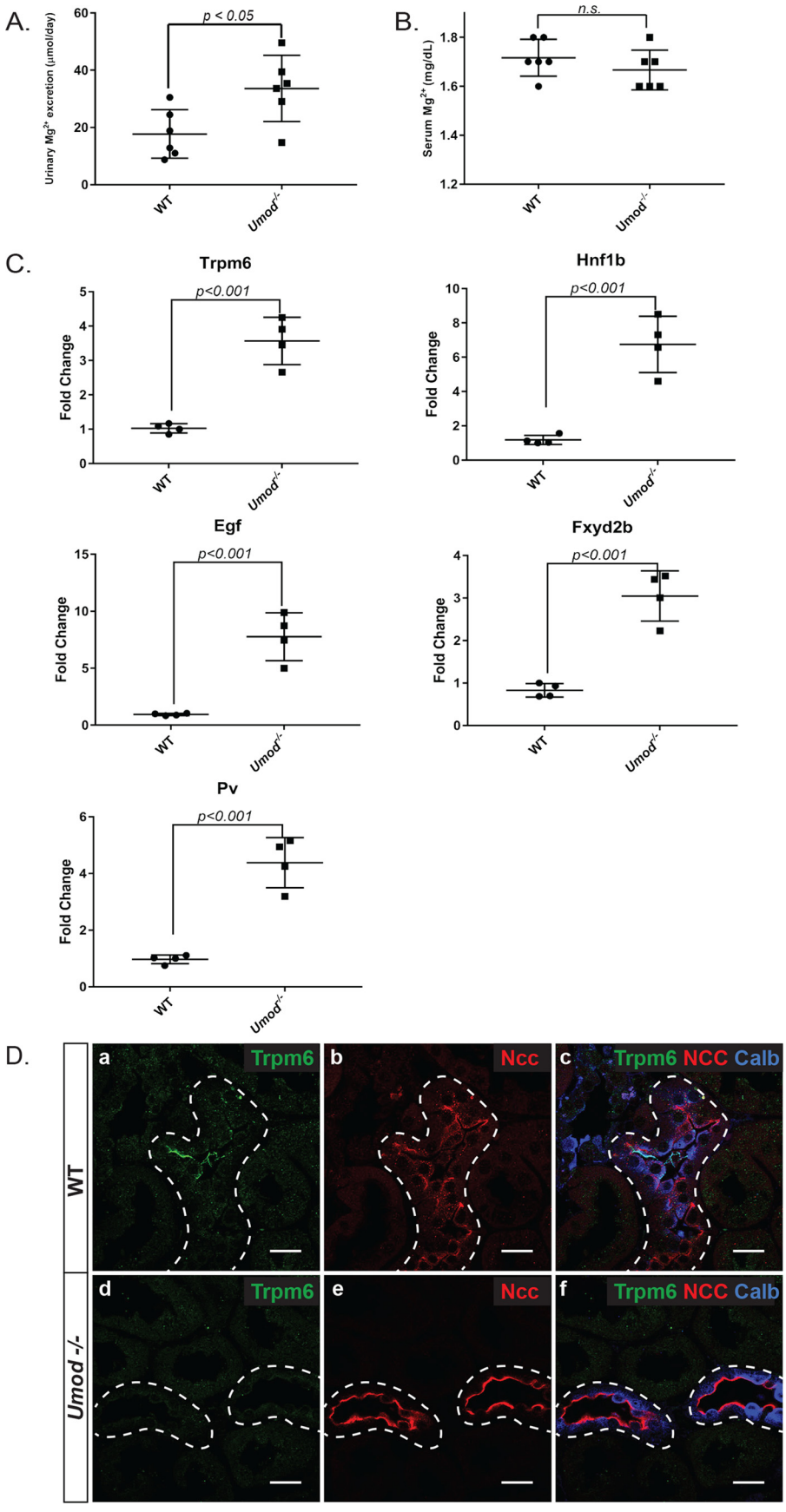
A.
Urinary Mg2+ excretion (µmol/day)
p < 0.05
WT
Umod-/-
B.
Serum Mg2+ (mg/dL)
n.s.
C.
Trpm6
p<0.001
Fold Change
Hnf1b
Egf
Fxyd2b
Pv
D.
WT
Umod -/-
a Trpm6
b Ncc
c Trpm6 NCC Calb
d Trpm6
e Ncc
f Trpm6 NCC Calb

Table 1

Urine and serum chemistries of 9-month-old WT and *Umod*$^{-/-}$ mice at baseline and after furosemide treatment

WT and *Umod*$^{-/-}$ mice were kept in metabolic cages. Urine was obtained by bladder massage. Data showing the change after furosemide challenge for WT and *Umod*$^{-/-}$ mice (in columns five and six) are shown as percentage from baseline obtained before furosemide challenge and 4 h after furosemide treatment. Data are normalized per hour. WT and *Umod*$^{-/-}$ mice did not respond significantly differently to furosemide challenge regarding urine output, urinary Na^+ excretion, K^+ excretion, Ca^{2+} excretion, or Mg^{2+} excretion. Data show mean ± S.D., $n = 14$ for each group. * in *Umod*$^{-/-}$ column, $p < 0.05$; # in *Umod*$^{-/-}$ column, $p < 0.01$ compared with WT column. § in WT + furosemide column, $p < 0.005$ compared with WT column. $ in WT + furosemide column, $p < 0.0001$ compared with WT column. $ in *Umod*$^{-/-}$ + furosemide column, $p < 0.0001$ compared with *Umod*$^{-/-}$ column. § in *Umod*$^{-/-}$ + furosemide column, $p < 0.005$ compared with *Umod*$^{-/-}$ column. Hct, hematocrit. ND, not determined.

	WT	*Umod*$^{-/-}$	WT + furosemide	*Umod*$^{-/-}$ + furosemide	Change in WT after furosemide	Change in *Umod*$^{-/-}$ after furosemide
					%	%
Weight (g)	41.1 ± 8.6	39.9 ± 4.3	38.3 ± 8.2	38 ± 3.3	−9.1 ± 5.5	−9.5 ± 4.6
Urine volume (μl/h)	43.6 ± 16.2	39.5 ± 13.8	621 ± 260$	731 ± 233$	1363 ± 308	1654 ± 396
Urinary excretion						
Na^+ (μmol/h)	6.4 ± 3.7	8.1 ± 3.2	75.9 ± 25.2$	98.3 ± 32.8$	1143 ± 263	1200 ± 186
K^+ (μmol/h)	11.1 ± 4.2	10.5 ± 4.5	37.6 ± 7.5§	50.5 ± 10.1$	353 ± 186	503 ± 155
Ca^{2+} (μmol/h)	0.24 ± 0.12	0.42 ± 0.1*	2.6 ± 0.9§	4.12 ± 1.3$	1184 ± 302	1059 ± 324
Mg^{2+} (μmol/h)	0.67 ± 0.15	1.45. ± 0.38#	7.58. ±3.2§	12.74 ± 4.5$	1139 ± 182	893 ± 174
Serum						
Hct (%)	48.4 ± 4.3	49.8 ± 5.2	50.5 ± 3.8	51.2 ± 3.3	ND	ND
Na^+ (mmol/L)	152.3 ± 1.6	152.7 ± 2.3	ND	ND	ND	ND
K^+ (mmol/liter)	4.92 ± 0.2	5.05 ± 0.6	ND	ND	ND	ND
Ca^{2+} (mmol/liter)	2.68 ± 0.06	2.74 ± 0.18	ND	ND	ND	ND
Mg^{2+} (mmol/liter)	0.8 ± 0.09	0.77 ± 0.13	ND	ND	ND	ND
Creatinine (mg/dl)	0.066 ± 0.014	0.078 ± 0.005	ND	ND	ND	ND

enhances TRPM6 current density through an extracellular, apical interaction within tubules.

UMOD up-regulation requires almost all UMOD domains except the GPI anchor

UMOD secondary structure contains an N-terminal leader peptide that is crucial for secretion of UMOD, followed by four EGF-like domains that are important for protein–protein interaction, a D8C cysteine-rich sequence of unknown significance, a zona pellucida (ZP) domain that is crucial for UMOD multimerization, and finally a GPI anchor domain (Fig. 4*A*). To determine which UMOD domain is required for TRPM6 up-regulation, we created different UMOD constructs and tested their effect on TRPM6 current density. Protein expression of different plasmids was assayed by Western blotting and titrated so that there was an equivalent amount of UMOD proteins in each condition. Full-length WT UMOD up-regulated TRPM6, whereas C150S mutant UMOD did not change TRPM6 current density compared with control (Fig. 4*B*). UMOD plasmids containing the EGF-like domains (L180X) or the EGF-like domains plus the D8C domains (C297X) had no effect on TRPM6 current density. However, the UMOD construct containing the EGF-like, D8C, and ZP domains (R586X) increased TRPM6 current density significantly (Fig. 4*B*). The ZP domain is essential and sufficient for formation of UMOD polymers (56). Our results show that the EGF-like, D8C, and ZP domains are required for TRPM6 up-regulation and suggest that UMOD multimerization may be involved in TRPM6 up-regulation (Fig. 4*B*).

UMOD physically interacts with TRPM6

To study whether UMOD interacts physically with TRPM6, we performed co-immunoprecipitation experiments in HEK293 cells transfected with HA-tagged UMOD, TRPM6, and GFP-tagged TRPM6. Using anti-HA to immunoprecipitate HA-tagged UMOD, we co-immunoprecipitated TRPM6 (Fig. 5*A*). Conversely, anti-GFP antibody immunoprecipitated GFP-tagged TRPM6 and co-immunoprecipitated HA-tagged UMOD (Fig. 5*B*, *fourth lane*). Immunoprecipitation of GFP alone did not show any interaction with UMOD (Fig. 5*B*, *third lane*). These experiments are consistent with a physical interaction between UMOD and TRPM6.

UMOD enhances TRPM6 current density by impairing TRPM6 endocytosis

Because our data were in line with an extracellular role of UMOD in TRPM6 up-regulation, we tested the hypothesis that UMOD may influence TRPM6 at the cell surface by interfering with TRPM6 endocytosis by studying the role of dynamin-2, a crucial protein for protein retrieval from the cell membrane. Expression of dynamin-2 in the DCT was described (57). When cells were co-transfected with WT dynamin-2, TRPM6 current density was up-regulated by UMOD (Fig. 6*A*). Cells co-transfected with dominant-negative (DN) dynamin-2, which impairs constitutive endocytosis, displayed enhanced TRPM6 current density even without UMOD (Fig. 6*A*). Stimulation of DN dynamin-2–transfected cells with UMOD did not result in any further increase of TRPM6 current density, indicating that

Figure 1. *Umod*$^{-/-}$ mice display urinary Mg^{2+} wasting and decreased tubular apical abundance of TRPM6. *A*, *Umod*$^{-/-}$ mice had almost twice the urinary Mg^{2+} excretion as control mice (WT 17.75 ± 8.47 μmol/24 h *versus* *Umod*$^{-/-}$ 33.63 ± 11.58 μmol/24 h, $p < 0.05$, $n = 6$ for each group). The results are representative of two experiments (see Table 1 with $n = 14$ for each group). *B*, despite higher urinary Mg^{2+} excretion in *Umod*$^{-/-}$ mice they have no lower serum Mg^{2+} (WT 1.72 ± 0.08 mg/dl *versus* *Umod*$^{-/-}$ 1.67 ± 0.08 mg/dl, not significant (*n.s.*), $n = 6$ for each group). The results are representative of two similar experiments. *C*, compared with WT mice, in *Umod*$^{-/-}$ mice, mRNA expression of genes involved in Mg^{2+} regulation, such as *Trpm6*, *Hnf1b*, *Egf*, *Fxyd2b*, and PV, were up-regulated, consistent with a Mg^{2+}-deficient state ($n = 4$ for each group). *D*, Trpm6, Ncc, and calbindin immunostaining in the mouse renal cortex. *a–c*, tubular apical staining of Trpm6 (*green*), Ncc (*red*; a marker of DCTs), and cytosolic calbindin-D28K (*blue*) expression in WT mice. Compared with WT mice, *Umod*$^{-/-}$ mice (*d–f*) had less apical Trpm6 abundance, whereas Ncc and calbindin-D28K expression remain unchanged and confirm the correct location of the DCT (*e* and *f*). *Scale bar*, 20 μm.

UMOD increases TRPM6 by interfering with dynamin-2–dependent TRPM6 endocytosis. This conclusion is further supported by experiments using dynasore, an inhibitor of dynamin GTPase activity and blocker of dynamin-dependent endocytosis (58) (Fig. 6*B*).

Previously, we have shown that the urinary protein Mucin-1 (MUC1) requires additional urinary proteins, such as galectin-3, a urinary lectin, for MUC1-related stimulation of the renal calcium channel TRPV5 (59). Galectins form a group of 15 members and bind β-galactosides (60, 61). We tested the hypothesis that galectin-3 also is a mediator of TRPM6 up-regulation by UMOD. We used an siRNA knockdown approach that is efficient in reducing endogenous galectin-3 protein expression as previously described (59). However, galectin-3

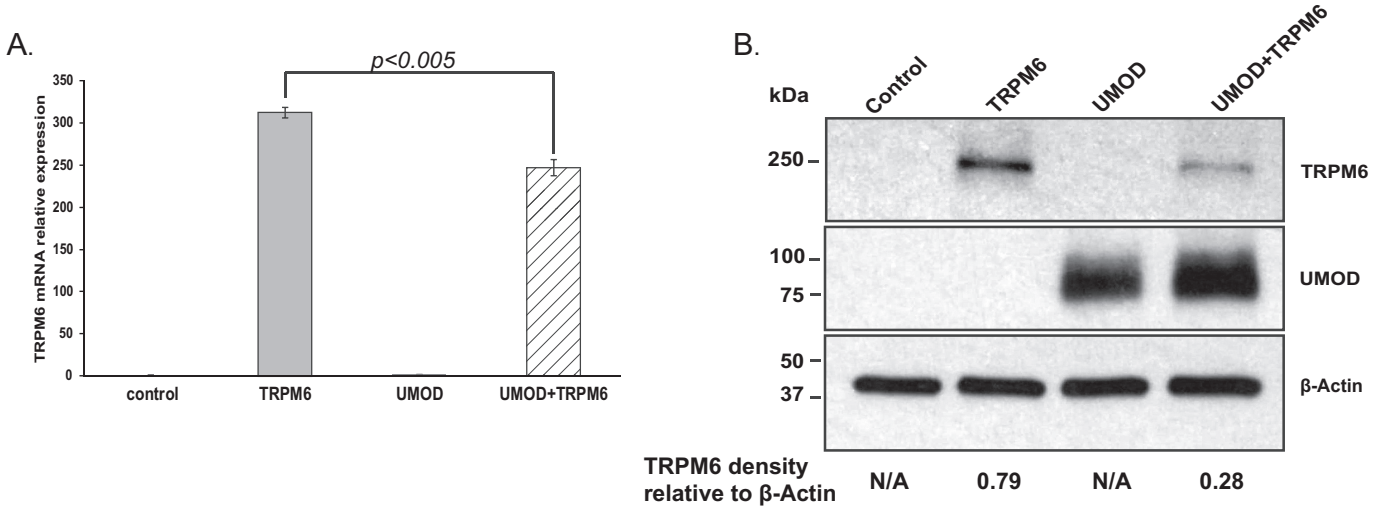

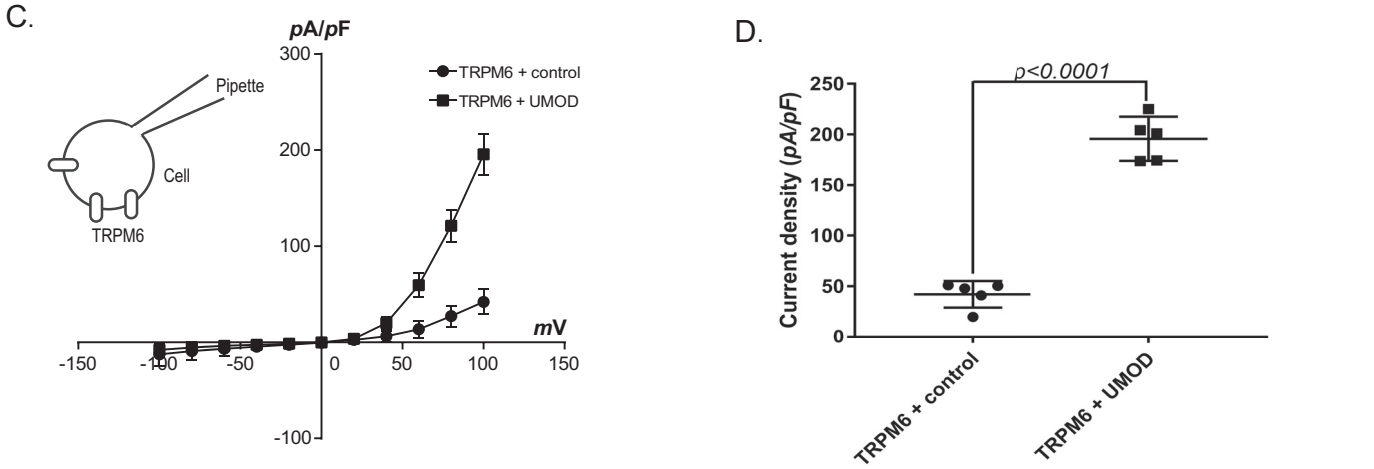

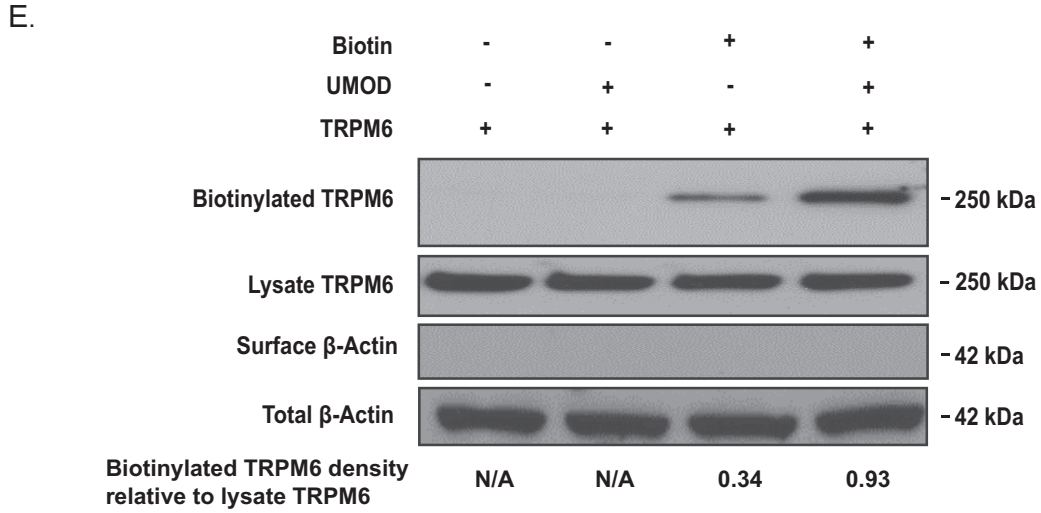

siRNA had no effect on TRPM6 current density up-regulation by UMOD, indicating that galectin-3 is not required for UMOD up-regulation of TRPM6 (Fig. 6*C*).

Another candidate for TRPM6 regulation by UMOD was galectin-1, which, like galectin-3, is a constituent of large cross-linked complexes that form lattice networks (62, 63). Galectin-1 forms homodimers and binds to TRPV5 *N*-glycan. Klotho, an antiaging hormone that also functions as a sialidase and modifies a variety of ion channels, enhances TRPV5 current density in a galectin-1–dependent fashion (63). In previous work (59), we demonstrated efficient reduction of endogenous galectin-1 protein applying an siRNA approach. We found that knockdown of galectin-1 abolished the stimulatory effect of UMOD toward TRPM6, consistent with an important role in UMOD-mediated TRPM6 up-regulation (Fig. 6*D*).

Because galectin-1 binds to *N*-glycans and UMOD-mediated up-regulation of TRPV5 requires the TRPV5's *N*-glycan, we wondered whether TRPM6 is also *N*-glycosylated. Using computational tools, we identified 17 potential *N*-glycosylation sites within the TRPM6 protein (64). We focused on the TRPM6 Asn-787 *N*-glycan site because it is the only *N*-glycan located in an extracellular loop of TRPM6, thus allowing extracellular proteins to interact with this *N*-glycan. We analyzed the effect of UMOD on WT and *N*-glycan– deficient TRPM6. In contrast to its effect on WT TRPM6, UMOD did not enhance current density of *N*-glycan– deficient N787A TRPM6, consistent with a role for the presumed TRPM6 *N*-glycan in UMOD up-regulation (Fig. 6*E*).

Urinary UMOD secretion is increased in low-Mg^{2+} states

As UMOD modified TRPM6 current density, we wondered whether a low-Mg^{2+} state itself could modify urinary UMOD secretion. In humans, urinary UMOD secretion is modified by dietary salt intake and antidiuretic and thyroid hormones (65–68). We placed WT mice first on a regular Mg^{2+} diet for 2 weeks and evaluated 24-h urinary UMOD secretion. Subsequently, the same animals were fed a low (50 ppm)-Mg^{2+} diet for 2 weeks, and 24-h urinary UMOD secretion was measured. The 24-h urine sample was studied by semiquantitative Western blotting, and tested urine volume was normalized to urine creatinine. Our studies showed that animals fed a low-Mg^{2+} diet had a significantly elevated, 2-fold stronger, urinary UMOD protein band compared with urine obtained on a regular diet (Fig. 7, *A* and *B*). These data are consistent with the systemic Mg^{2+} state influencing the urinary UMOD secretion and point toward a feedback mechanism targeting systemic Mg^{2+} homeostasis.

Discussion

The majority of filtered Mg^{2+} is absorbed in the TAL (50–70%) in a paracellular fashion due to the lumen-positive potential that is created by electroneutral absorption of Na^+, K^+, and 2 Cl^- via NKCC2 and subsequent K^+ secretion through ROMK back into the lumen (26). UMOD has been shown to up-regulate NKCC2 and ROMK and is therefore thought to contribute to Mg^{2+} absorption in the TAL (44, 45, 69, 70).

Our data are consistent with an additional role for UMOD in Mg^{2+} absorption in the DCT. This is the first study to show that UMOD from the extracellular space can directly stimulate the cell-surface abundance of TRPM6 channels and thus enhances TRPM6 current density. In our model, UMOD is secreted from the TAL and up-regulates TRPM6 channels in the DCT from the urinary space by forming a carbohydrate lattice with a newly identified TRPM6 *N*-glycan (Fig. 8). Lattice formation requires galectin-1 and interferes with TRPM6 endocytosis, thereby increasing the TRPM6 cell-surface abundance and allowing for enhanced tubular Mg^{2+} absorption to compensate for low-Mg^{2+} states.

Published data on urinary Mg^{2+} excretion in *Umod*$^{-/-}$ mice has been ambiguous. Mo *et al.* (43) showed no increase in urinary Mg^{2+} excretion in 2–3-month-old *Umod*$^{-/-}$ mice, but Liu *et al.* (71) described increased urinary Mg^{2+} excretion at 5–8 months of age. However, in a recent publication, the same group reports high urinary Mg^{2+} excretion in 1-month-old *Umod*$^{-/-}$ mice and a lower degree of urinary Mg^{2+} wasting in 12-month-old *Umod*$^{-/-}$ animals (46). It is possible that these results are conflicting because urinary Mg^{2+} concentration was assessed rather than a measurement of urinary Mg^{2+} excretion (*e.g.* correction for urinary volume and collection time). Our results, which were performed at 5 and 9 months of age, show higher urinary Mg^{2+} and Ca^{2+} excretion (*e.g.* corrected for volume and time) in the *Umod*$^{-/-}$ mice compared with control mice (Fig. 1*A*, Table 1, and Table S1).

UMOD has been shown to up-regulate NKCC2 and ROMK in the TAL (44, 45, 69, 70). Mutig *et al.* (45) and Liu *et al.* (46) also demonstrated a blunted response in *Umod*$^{-/-}$ mice after furosemide treatment, supporting the hypothesis of a defective TAL in *Umod*$^{-/-}$ mice. Therefore, our finding that 9-month-old WT and *Umod*$^{-/-}$ mice responded in a similar fashion to furosemide was unexpected (Table S1 and Table 1). We considered that there may be a different response to furosemide dependent on the age of the *Umod*$^{-/-}$ mice, given the fact that most published furosemide challenges in *Umod*$^{-/-}$ mice were performed at 3 months (45, 69, 70). However, 5- and 9-month-

Figure 2. UMOD enhances TRPM6 whole-cell current density and TRPM6 apical cell-surface abundance but not TRPM6 mRNA or protein. *A*, we compared TRPM6 mRNA expression in HEK293 cells when co-transfected with control or UMOD using quantitative RT-PCR. TRPM6 mRNA expression was not increased with UMOD co-transfection. Experiment was repeated in triplicate. *B*, Western blotting of TRPM6 protein expression at 48 h after co-transfection with control or UMOD. TRPM6 protein was not increased when co-transfected with UMOD. TRPM6 protein band density relative to β-actin is shown *below*. The experiment was repeated in triplicate. *C*, in HEK293 cells, co-expression of TRPM6-GFP with WT UMOD for 48 h increased the TRPM6 current density compared with control (196 ± 22 pA/pF *versus* 42 ± 13 pA/pF, $p < 0.0001$). TRPM6 current density (current normalized to cell-surface area, pA/pF; mean ± S.D. (*error bars*)) was evoked by test pulses from −100 to 100 mV, with +20-mV increments for 400 ms. The steady-state current–voltage (*I-V*) relation curve showed characteristic outwardly rectifying TRPM6 currents in cells co-transfected with TRPM6 with control *versus* UMOD ($n = 5$ for each group). The experiment was performed in triplicate. *D*, scatter plot shows TRPM6 current density (pA/pF) at +100 mV co-transfected with control or UMOD. *E*, UMOD effect on TRPM6 cell-surface abundance measured by biotinylation assay. TRPM6 abundance at plasma membrane (*top*) and total lysates (*middle*) were analyzed by immunoblot analysis using antibody against TRPM6. The antibody did not detect protein signal in the untransfected cells (data not shown). For detection of TRPM6 in the surface (biotinylated TRPM6, *top row*) and lysate (lysate TRPM6, *second row*), 250 and 20 μg of protein were separated by SDS-gel electrophoresis, respectively. The experiment was repeated in duplicate. *N/A*, not applicable.

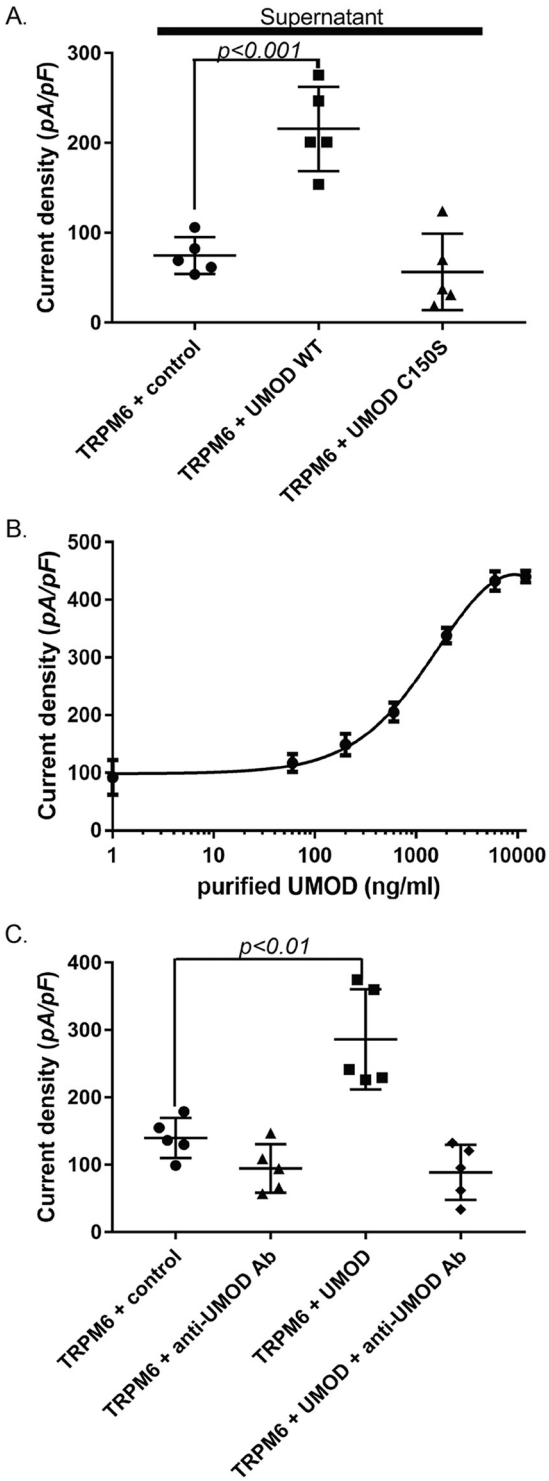

Figure 3. UMOD enhances TRPM6 current density from the extracellular space in a dose-dependent fashion. *A*, HEK293 cells were transfected with control, WT UMOD, or C150S UMOD (a human *UMOD* mutation that reduces urinary UMOD secretion as previously shown by us (52)). 48 h later, the supernatant containing control, WT UMOD, or C150S UMOD was collected. The harvested supernatant was placed on separately cultured cells transfected with TRPM6 and cultured overnight. The scatter plot shows TRPM6 current density at +100 mV for supernatant containing control, WT UMOD, and C150S UMOD (75 ± 21 *versus* 216 ± 47 *versus* 56 ± 42 pA/pF, $p < 0.001$) (n = 5 for each group). *B*, increasing concentrations of purified UMOD (final concentration in the medium is shown) enhanced TRPM6 current density in a dose-dependent fashion. TRPM6-transfected cells were treated with purified UMOD overnight. *C*, effect of anti-UMOD antibody (*anti-UMOD Ab*) on TRPM6 up-regulation by purified UMOD. Anti-UMOD antibody was added to culture medium of cells transfected with TRPM6 and treated with control or purified UMOD (n = 5 for each group). All experiments in Fig. 3 were performed in triplicate. *Error bars*, S.D.

old WT and *Umod*$^{-/-}$ animals showed a very similar response to furosemide, thus limiting the possibility of an age-dependent furosemide response in *Umod*$^{-/-}$ mice. A number of other experimental variables may account for the observed differences to furosemide in *Umod*$^{-/-}$ mice, such as genetic background, different *Umod*$^{-/-}$ mouse model, mouse strain, furosemide dose, urine collection method, and correction for urine volume or body weight. Consistent with our previous data on UMOD-mediated enhancement of TRPV5 cell- surface abundance, the 9-month-old *Umod*$^{-/-}$ mice had hypercalciuria, and there was a clear trend to higher urinary calcium excretion in the 5-month-old *Umod*$^{-/-}$ animals (Table 1 and Table S1) (52). Including our other experiments, our results are consistent with an effect of UMOD in the DCT. Finally, a recent publication describes a smaller degree (10–15% compared with TAL) of UMOD secretion in the DCT (72).

Galectin-1 expression was demonstrated in the urogenital tract of mice and humans, and it is a key player for Klotho-mediated modification of ROMK and TRPV5 cell-surface abundance (63, 73–75). Klotho functions as a α-2,6-sialidase, thereby removing specific terminal sialic acid residues from the channel's *N*-glycan. Galectin-1 then binds to the underlying disaccharide GlcNAc, thus contributing to lattice formation. Galectin-1 could either stabilize the UMOD mulitmerization or promote the interaction between TRPM6 and UMOD. Similar regulation by urinary proteins was described for other apical tubular ion channels, such as ROMK and TRPV5, by UMOD, MUC1, tissue kallikrein, and Klotho (52, 59, 63, 73, 76).

UMOD is the most abundant protein in urine. Our estimated EC_{50} for UMOD-mediated up-regulation of TRPM6 current density is 10-fold higher than for TRPV5, but significantly lower than the estimated UMOD concentration in the DCT, suggesting near-maximally active TRPM6 channels in most conditions (52). We think that our results are more within the dynamic range of UMOD concentrations, as UMOD has to multimerize via the ZP domains (Figs. 4 and 8) to increase TRPM6 current density, and because we expect the effective concentration of macromolecular UMOD to be lower than that of UMOD monomers.

Interestingly, although serum Mg^{2+} concentration in *Umod*$^{-/-}$ mice was not appreciably changed, several genes promoting Mg^{2+} absorption were up-regulated (Fig. 1*C*). Measurement of serum Mg^{2+} is known to be an insensitive marker of systemic Mg^{2+} status, as only about 1% of total body Mg^{2+} is in the extracellular fluid, with the remainder equally distributed in bone and soft tissue (77–80). Our results are similar to those of another study showing up-regulated colonic Trpm6 mRNA but no effect on serum Mg^{2+} concentration in mice fed omeprazole, a proton pump inhibitor that causes Mg^{2+} deficiency, or a low-Mg^{2+} diet (81, 82). A recent publication (38) suggested that urinary Mg^{2+} excretion in humans may be a better marker of disturbed Mg^{2+} homeostasis. One may wonder how the *Umod*$^{-/-}$ mice maintain a normal serum

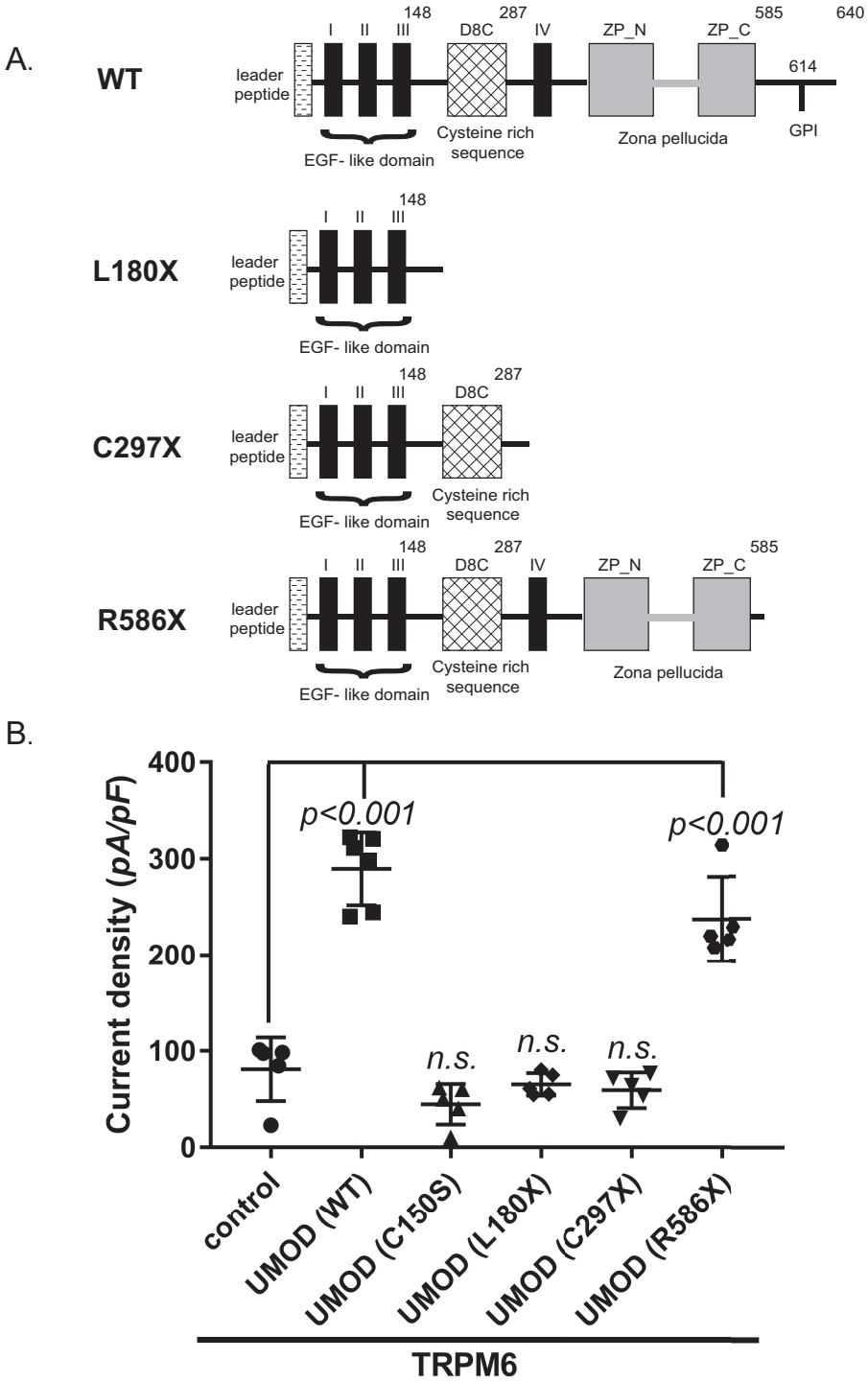

Figure 4. The EGF-like, D8C, and ZP domains of UMOD are required for up-regulation of TRPM6. *A*, UMOD contains a leader peptide, which is important for proper secretion of UMOD; four (*I–IV*) EGF-like domains, which are crucial for protein–protein interaction; a D8C domain, which is enriched with cysteine residues and of unknown significance; and the ZP domain, which is required for UMOD multimerization. For UMOD secreted into urine, all three protein domains could be important, as UMOD is cleaved at the C terminus between the ZP domain and the GPI anchor. We created deletion constructs with a premature stop after the EGF-like (L180X), the D8C domain (C297X), and the ZP domains (R586X). Amino acids are provided *above* the model for the protein domains. *B*, co-transfection of TRPM6 and WT UMOD confirmed the up-regulation of TRPM6 current density in contrast to control or UMOD C150S mutant. The plasmids containing only the EGF-like (UMOD L180X) or the EGF-like plus D8C domains (UMOD C297X) had no effect on TRPM6 current density. Only the plasmid containing all three major domains (the EGF-like, D8C, and ZP domains) but not the GPI anchor (UMOD R586X) was able to increase TRPM6 current density in a significant fashion. Protein expression of different plasmids was assayed by Western blotting and titrated so that there was an equivalent amount of UMOD proteins in each condition ($n = 5$ for each group). The experiment was performed in duplicate.

Mg^{2+} concentration despite increased urinary Mg^{2+} excretion. Probably, there are redundant renal and nonrenal mechanisms to ensure Mg^{2+} homeostasis in *Umod*$^{-/-}$ mice, as Trpm6 is also localized in the cecum and colon (34, 81). Therefore, frank hypomagnesemia may only occur with the challenge of a low-Mg^{2+} diet. Mg^{2+} depletion alone was reported to enhance

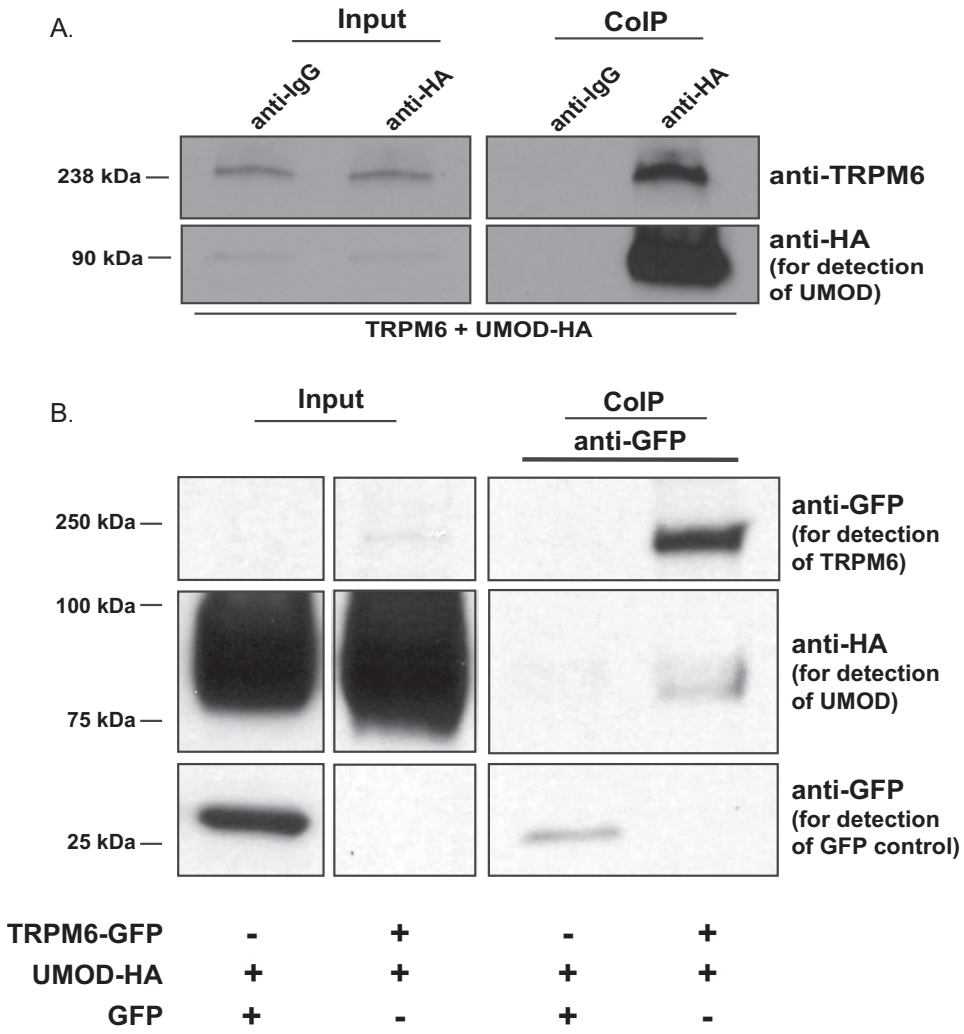

Figure 5. UMOD binds physically to TRPM6. *A*, HEK293 cells were transiently transfected with UMOD-HA and TRPM6. The antibody used for immunoprecipitation is shown *above* each *panel* (*CoIP*). Immunoprecipitated proteins were identified using Western blotting (*WB*) and specific antibodies as shown on the *right*. Cell lysate is shown at the *left* of each immunoprecipitation experiment. 400 μg of lysate was used for immunoprecipitation, and 4 μg of protein was loaded for input. TRPM6 is detected with precipitation of the UMOD–TRPM6 complex using anti-HA antibody (*lane 4*). *B*, to confirm UMOD–TRPM6 physical interaction, we transfected either GFP or TRPM6-GFP with UMOD. Anti-GFP antibody was used for immunoprecipitation. Immunoprecipitated proteins were identified using Western blotting and specific antibodies as shown on the *right*. 400 μg of lysate was used for immunoprecipitation, and 8 μg of protein was loaded for input. Cell lysate is shown at the *left* of each immunoprecipitation experiment. Whereas GFP (25 kDa) as a negative control did not precipitate with UMOD (*lane 3*), UMOD-HA was detected with precipitation of the UMOD-HA–TRPM6-GFP complex. Samples for UMOD and GFP input (*B*, *left*) were run on the same Western blot as the remaining samples but not adjacent to each other. Therefore, they are separated by *white bars*. Both experiments were performed in duplicate.

renal Trpm6, PV, and Hnf1b mRNA expression in WT mice (34, 82). Increased mRNA gene expression of these genes points toward a compensatory mechanism to cope with a low-Mg^{2+} state.

It is tempting to consider that some of the complications of chronic hypomagnesemia could be due to TRPM6 dysregulation caused by insufficient UMOD secretion in low-Mg^{2+} states. Remarkably, similar to hypomagnesemia, either low serum or urinary UMOD concentrations have been associated with a higher risk of cardiovascular disease, type 2 diabetes mellitus, and nephrolithiasis (21, 83–85). Interestingly, the degree of UMOD secretion depends on specific SNPs in *UMOD* and the *UMOD* promoter (44, 86, 87). Individuals carrying SNPs resulting in a reduced baseline UMOD secretion may have an impaired ability to respond appropriately to low-Mg^{2+} states with increased urinary UMOD secretion. This would expose carriers of such *UMOD* SNPs to chronic, mild to moderate hypomagnesemia and subsequent complications.

Experimental procedures

Materials and DNA constructs

UMOD purified from human urine was purchased from SunnyLab (Sittingbourne, UK). The rabbit polyclonal anti-GFP-peroxidase antibody was obtained from Invitrogen/Molecular Probes, Inc. (Eugene, OR). Human TRPM6 was cloned into the bicistronic vector pCINeo/IRES-GFP (32). TRPM6 N787A was obtained from WT TRPM6 using the XL site-directed mutagenesis kit from Agilent (Santa Clara, CA). To test the predicted N787A TRPM6 *N*-glycan site, WT and N787A TRPM6 were subcloned into pcDNA DEST53, which contains a GFP tag (Thermo Fisher Scientific). Protein G immobilized on agarose, mouse monoclonal anti-HA anti-

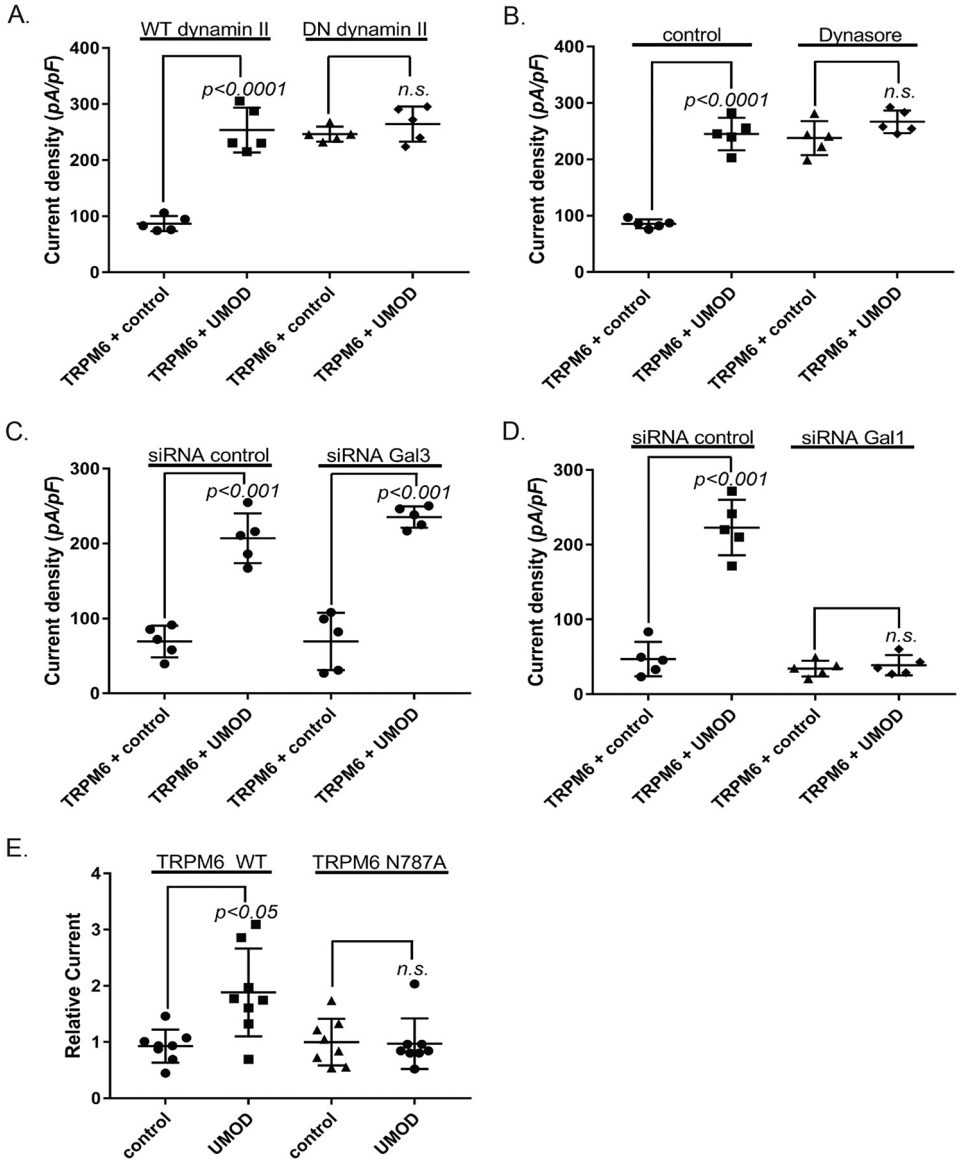

Figure 6. UMOD up-regulates TRPM6 together with endogenous galectin-1 by impairing dynamin-2–dependent TRPM6 endocytosis. *A*, UMOD increases TRPM6 current density by impairing dynamin-2–dependent endocytosis of the channel. Whereas cells transfected with WT dynamin-2 showed the expected up-regulation of TRPM6 current density with UMOD (for WT dynamin-2: 87 ± 13 pA/pF with control *versus* 254 ± 40 pA/pF with UMOD, $p < 0.0001$), cells transfected with DN dynamin-2 displayed increased TRPM6 current density at baseline, indicating constitutive TRPM6 endocytosis by dynamin-2. In these cells, no further increase of TRPM6 activity was found with UMOD (for DN dynamin-2: 246 ± 13 pA/pF with control *versus* 265 ± 31 pA/pF with UMOD, not significant (*n.s.*)), indicating that TRPM6 up-regulation by UMOD occurs by impairing dynamin-2–dependent endocytosis. *B*, confirmation of UMOD up-regulation of TRPM6 by impairing dynamin-dependent TRPM6 endocytosis using dynasore. Using the dynamin GTPase inhibitor dynasore, which blocks dynamin-dependent endocytosis, we confirmed the lack of UMOD effect on TRPM6 current density (no dynasore: 86 ± 8 pA/pF with control *versus* 245 ± 29 pA/pF with UMOD, $p < 0.0001$; plus dynasore: 238 ± 30 pA/pF with control *versus* 267 ± 20 pA/pF with UMOD, not significant). *C*, galectin-3 is not required for TRPM6 up-regulation by UMOD. Knockdown of galectin-3 using siRNA (performed as previously described by us (59)) did not impair the response of TRPM6 current density to UMOD (control siRNA: 69 ± 21 pA/pF with control *versus* 207 ± 33 pA/pF with UMOD, $p < 0.001$; galectin-3 siRNA: 69 ± 38 pA/pF with control *versus* 235 ± 14 pA/pF with UMOD, $p < 0.001$). *D*, knockdown of galectin-1 (performed as previously described by us (59)) abrogates up-regulation of TRPM6 current density by UMOD (control siRNA: 47 ± 23 pA/pF with control *versus* 223 ± 37 pA/pF with UMOD, $p < 0.01$; galectin-1 siRNA: 34 ± 11 pA/pF with control *versus* 39 ± 14 pA/pF with UMOD, not significant). Efficiency of siRNA for galectin-1 and galectin-3 was shown previously (59). *E*, the predicted Asn-787 *N*-glycan of TRPM6 is required for up-regulation by UMOD. WT TRPM6 responded to UMOD co-transfection (relative current WT TRPM6: 0.92 ± 0.29 with control *versus* 1.88 ± 0.78 with UMOD, $p < 0.05$), whereas *N*-glycan–deficient (N787A) TRPM6 did not react to UMOD stimulation (relative current N787A TRPM6: 1 ± 0.42 with control *versus* 0.97 ± 0.45 with UMOD, not significant). For experiments shown in *A–D*, sample size was $n = 5$ for each group, and experiments were performed in triplicate. For the experiment shown in *E*, sample size was $n = 8$ for each group, and the experiment was performed in triplicate. *Error bars*, S.D.

body, and mouse monoclonal anti-β-actin-peroxidase antibody were purchased from Sigma. Cappel antibody against human uromucoid (Tamm–Horsfall glycoprotein) from goat was purchased from MP Biochemicals (Solon, OH). Donkey antibody against goat IgG was obtained from Santa Cruz Biotechnology, Inc. (Dallas, TX).

Cell culture and transfection

HEK293 cells were cultured as described (88). Cells were transiently transfected using Lipofectamine 2000® reagent (Thermo Fisher Scientific) with plasmids (2 μg per well in a 6-well plate) containing GFP-TRPM6, WT UMOD, or C150S mutant UMOD

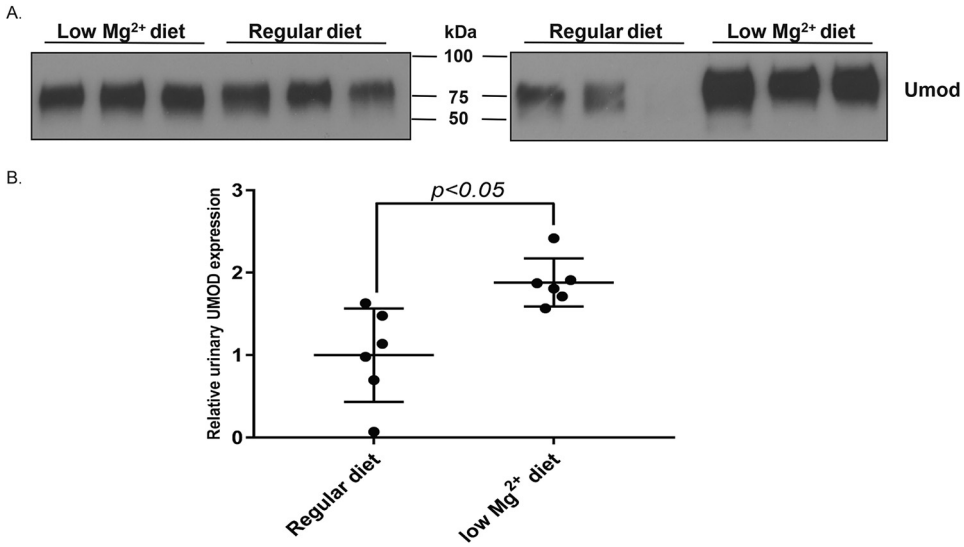

Figure 7. Urinary Umod is increased in mice fed a low-Mg^{2+} diet. *A*, mice fed with low-Mg^{2+} diet for 2 weeks excreted more urinary UMOD than animals fed with a regular diet. Studied urine volume was normalized to urine creatinine ($n = 6$ for each group). *B*, comparison of UMOD protein band density in WT animals fed a regular diet and low-Mg^{2+} diet. Relative urinary UMOD secretion was significantly higher in WT mice provided a low-Mg^{2+} diet. The results are representative of two experiments. *Error bars*, S.D.

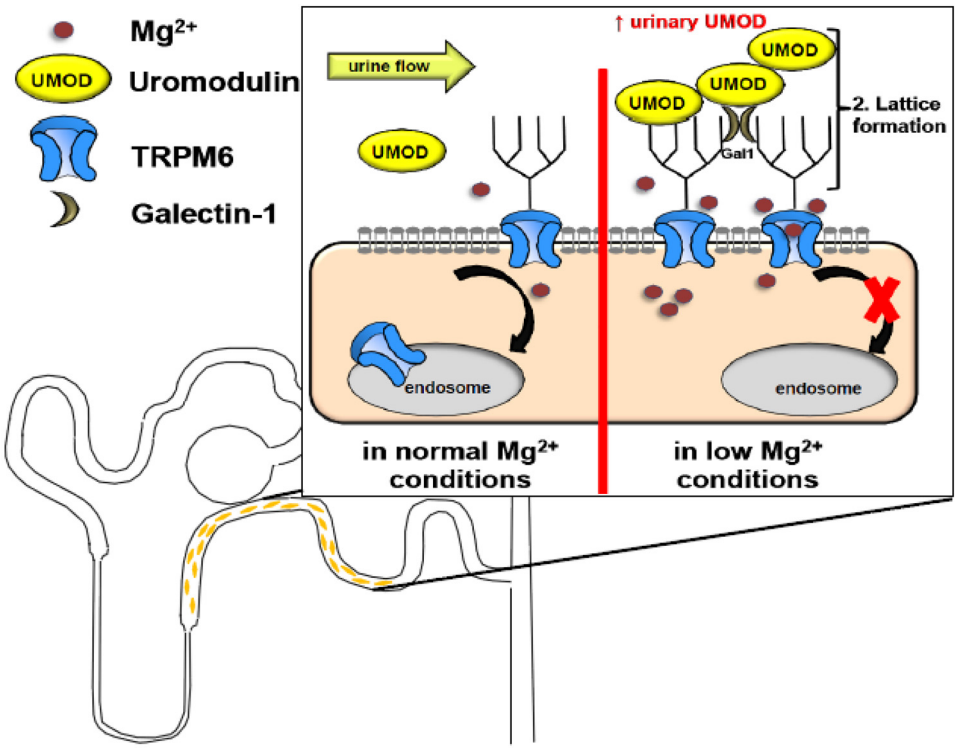

Figure 8. Model of TRPM6 regulation by UMOD. UMOD is secreted in the TAL. Urinary secretion of UMOD is enhanced in low-Mg^{2+} states. UMOD forms multimers through the ZP domains and interacts through a predicted *N*-glycan with TRPM6. Galectin-1 either stabilizes UMOD multimerization or UMOD–TRPM6 interaction, thus promoting lattice formation. The latter impairs dynamin-2–dependent endocytosis of TRPM6, thereby increasing the TRPM6 cell-surface abundance. This allows the nephron to compensate for low-Mg^{2+} states.

and WT or dominant-negative (K44A) rat dynamin II or control vectors, as indicated, in each experiment. In each experiment, the total amount of DNA for transfection was balanced by using empty vectors. For galectin-1 and galectin-3 siRNA (Dharmacon, Lafayette, CO) transfections, we utilized 40 and 20 nmol, respectively (59).

Quantitative RT-PCR studies

Total RNA was isolated from kidneys from WT and *Umod*$^{-/-}$ mice using miRNeasy Mini kits from Qiagen (Germantown, MD). First-strand cDNA was synthesized by an iScript™ cDNA synthesis kit (Bio-Rad). Relative transcript expression was measured by quantitative real-time PCR using iTaq™ Universal SYBR® Green Supermix (Bio-Rad). Samples were run on a CFX96 real-time PCR detection system (Bio-Rad). 18S RNA was used to normalize for expression of mRNA. Primers for quantitative RT-PCR were described previously (82). Data were analyzed using the Bio-Rad CXF software.

Whole-cell patch-clamp recording

In brief, whole-cell patch clamp recording, co-immunoprecipitation, and immunofluorescent studies were performed in a similar fashion as outlined previously (52, 59). Approximately 48 h after transfection, cells were dissociated and placed in a chamber for ruptured whole-cell recordings as described previously. Transfected cells were identified for recording by their GFP fluorescence. TRPM6 bath solution contained 140 mM NaCl, 5 mM CsCl, 2 mM $CaCl_2$, 1 mM $MgCl_2$, 10 mM glucose, 10 mM HEPES (pH 7.4 with NaOH). The pipette TRPM6 solution contained 120 mM CsCl, 10 mM NaCl, 1 mM HEDTA, and 10 mM HEPES (pH 7.2 with CsOH). Whole-cell patch clamp pipettes were pulled from borosilicate glass (Dagan Corp., Minneapolis, MN) and had resistance between 1.5 and 3 megaohms. The cell membrane capacitance and series resistance were monitored and compensated (>75%) electronically using an Axopatch 200B amplifier (Axon Instruments, Foster City, CA). The voltage protocol consists of a 0-mV holding potential and successive voltage sets (400-ms duration) from −100 to +100 mV in +20 increments. Current densities were obtained by normalizing current amplitude (obtained at +100 mV) to cell capacitance. Data acquisition was performed using ClampX version 9.2 software (Axon Instruments). Currents were low-pass filtered at 2 kHz using an 8-pole Bessel filter in the clamp amplifier, sampled every 0.1 ms (10 kHz) with the Digidata-1440 interface, and stored directly to a computer hard drive.

Surface biotinylation assay

Biotinylation studies were performed as outlined previously (52). Specifically, for biotinylation of cell-surface TRPM6, cells were washed with ice-cold PBS and incubated with 0.75 ml of PBS containing 0.75 mg/ml EZ-Link-NHS-SS-biotin (Thermo Scientific, Rockford, IL) for 1 h at 4 °C. After being quenched with glycine (100 mM), cells were lysed in radioimmune precipitation buffer (150 mM NaCl, 50 mM Tris-HCl, 5 mM EDTA, 1% (v/v) Triton X-100, 0.5% deoxycholate, and 0.1% (w/v) SDS) containing protease inhibitor mixture (Roche Applied Science). Biotinylated proteins were precipitated by streptavidin-agarose beads (Thermo Scientific). Beads were subsequently washed four times with PBS containing 1% (v/v) Triton X-100. Biotin-labeled proteins were eluted in sample buffer, heated at 50 °C for 5 min, separated by SDS-PAGE electrophoresis, and transferred to nitrocellulose membranes for Western blotting. TRPM6 proteins on the membrane were detected using a mouse monoclonal anti-TRPM6 (human) antibody (Santa Cruz Biotechnology). Biotinylation experiments were performed three times with similar results.

Co-immunoprecipitation and immunoblotting

HEK293 cells were co-transfected with HA-tagged UMOD and either TRPM6 or GFP-tagged TRPM6 using Lipofectamine 2000 and incubated for 48 h at 37 °C. Cells were collected and lysed using a needle syringe. The protein concentration in the cell lysate was determined using a protein assay (DC Protein Assay, Bio-Rad). Samples were adjusted to the same concentration with buffer. Samples were resolved on a 4–20% gradient gel and processed for immunoblotting using specific antibodies. For immunoprecipitations, we incubated 700 μg of cell lysate with 3 μg of anti-HA, anti-TRPM6, or anti-GFP antibodies overnight at 4 °C. Species-specific anti-IgG (Santa Cruz Biotechnology) was used as control. Antigen–antibody complex was then loaded onto Protein G beads (GE Healthcare, Little Chalfont, UK) by slow rotation overnight, washed, and eluted with Laemmli sample buffer. Samples were denatured at 65 °C for 10 min and subjected to SDS-PAGE and immunoblotting. Antibodies against human TRPM6 (Santa Cruz Biotechnology) and UMOD (MP Biochemicals, Solon, OH) were used for Western blotting.

Immunofluorescent staining

Male WT mice were sacrificed at the age of 3 months. Anesthetized mice were perfused with 4% (w/v) paraformaldehyde in PBS (pH 7.4). Kidneys were harvested and sectioned. Sections were blocked with 10% (v/v) donkey sera in PBS, and immunofluorescence was performed with guinea pig anti-Trpm6 antibody (1:50), mouse anti-calbindin-D28K (1:100), and rabbit anti-Ncc (1:200; Millipore) overnight at 4 °C (34). Fluorescent images were obtained using a Zeiss LSM510 confocal microscope (Zeiss, Jena, Germany). All animal experiments were performed in compliance with relevant laws and institutional guidelines and were approved by the University of Texas Southwestern Medical Center at Dallas Institutional Animal Care and Use Committee.

Metabolic cage studies in mice

Urinary excretion of Mg^{2+} was determined in 9-month-old WT and *Umod*$^{-/-}$ mice on a 129/SeEv background (43). Animals were acclimated for 3 days in metabolic cages before experiments. Daily urine volume was measured after bladder massage (89). Urine Mg^{2+} was analyzed by the University of Texas Southwestern metabolic phenotyping core. For furosemide challenge and urinary UMOD secretion studies, see the supporting information.

Furosemide challenge and urinary UMOD secretion in mice

Baseline 24-h urine collections were obtained. Complete bladder emptying was ensured by bladder massage. Animals were injected with a single dose of 15 mg/kg furosemide intraperitoneally (90). Urine was collected after 4 h with bladder massage (89). Urine output, sodium, potassium, calcium, and magnesium were analyzed by the University of Texas Southwestern metabolic phenotyping core. Furosemide response was assessed individually for every mouse by determining the hourly excretion of urine volume and electrolytes before and after furosemide treatment. To calculate the furosemide response, urinary data (*e.g.* volume and electrolyte excretion) obtained before and 4 h after treatment were corrected for collection time. For every individual animal, data points obtained after furosemide treatment were divided by the data points before treatment and multiplied by 100. To study the urinary UMOD secretion in mice, WT mice were fed a low (50 ppm)-Mg^{2+} diet (Teklad, TD.02073) for 2 weeks followed by 2 weeks of a regular diet. At the end of each dietary treatment, urine was collected as outlined above. Urine creatinine was determined by the University of Texas Southwestern O'Brien Kidney Center. Urine volume was normalized for urinary creatinine, and

UMOD secretion was studied in a semiquantitative fashion by Western blotting using anti-Thp (G-20) antibody (1:200) from Santa Cruz Biotechnology.

Statistical analysis

Student's *t* tests were used to test whether there are significant differences in the continuous outcomes between two study groups. For multiple comparisons, one-way analysis of variance studies followed by the Student-Newman-Keuls method, allowing for pairwise multiple comparisons, were performed. Data are reported as means ± S.D. $p < 0.05$ was considered statistically significant.

Author contributions—M. T. F. W., J. G. J. H., and R. J. M. B. designed the study. M. N. performed all of the cell culture work and protein biochemistry. M. S. B. performed whole-cell patch-clamp recording. J. L. and C. R. performed whole-animal physiology and TRPM6 cloning. Z. Y. and D. K. M. performed immunofluorescence studies. X.-R. W. provided *Umod*$^{-/-}$ mice. M. T. F. W. prepared the figures and wrote the manuscript, which was revised by all authors.

Acknowledgments—We greatly appreciate the scientific input from Drs. M. Baum, V. Patel, and A. Rodan.

References

1. Schimatschek, H. F., and Rempis, R. (2001) Prevalence of hypomagnesemia in an unselected German population of 16,000 individuals. *Magnes. Res.* **14,** 283–290 Medline
2. Pham, P. C., Pham, P. A., Pham, S. V., Pham, P. T., Pham, P. M., and Pham, P. T. (2014) Hypomagnesemia: a clinical perspective. *Int. J. Nephrol. Renovasc. Dis.* **7,** 219–230 Medline
3. Whang, R., and Ryder, K. W. (1990) Frequency of hypomagnesemia and hypermagnesemia: requested *vs* routine. *JAMA* **263,** 3063–3064 CrossRef Medline
4. Chernow, B., Bamberger, S., Stoiko, M., Vadnais, M., Mills, S., Hoellerich, V., and Warshaw, A. L. (1989) Hypomagnesemia in patients in postoperative intensive care. *Chest* **95,** 391–397 CrossRef Medline
5. Lopez-Ridaura, R., Willett, W. C., Rimm, E. B., Liu, S., Stampfer, M. J., Manson, J. E., and Hu, F. B. (2004) Magnesium intake and risk of type 2 diabetes in men and women. *Diabetes Care* **27,** 134–140 CrossRef Medline
6. Song, Y., Manson, J. E., Buring, J. E., and Liu, S. (2004) Dietary magnesium intake in relation to plasma insulin levels and risk of type 2 diabetes in women. *Diabetes Care* **27,** 59–65 CrossRef Medline
7. Pham, P. C., Pham, P. M., Pham, S. V., Miller, J. M., and Pham, P. T. (2007) Hypomagnesemia in patients with type 2 diabetes. *Clin. J. Am. Soc. Nephrol.* **2,** 366–373 CrossRef Medline
8. Kao, W. H., Folsom, A. R., Nieto, F. J., Mo, J. P., Watson, R. L., and Brancati, F. L. (1999) Serum and dietary magnesium and the risk for type 2 diabetes mellitus: the Atherosclerosis Risk in Communities Study. *Arch. Intern. Med.* **159,** 2151–2159 CrossRef Medline
9. Kurstjens, S., de Baaij, J. H., Bouras, H., Bindels, R. J., Tack, C. J., and Hoenderop, J. G. (2017) Determinants of hypomagnesemia in patients with type 2 diabetes mellitus. *Eur. J. Endocrinol.* **176,** 11–19 CrossRef Medline
10. Guerrero-Romero, F., Rodriguez-Moran, M., Hernandez-Ronquillo, G., Gomez-Diaz, R., Pizano-Zarate, M. L., Wacher, N. H., Mondragon-Gonzalez, R., and Simental-Mendia, L. E. (2016) Low serum magnesium levels and its association with high blood pressure in children. *J. Pediatr.* **168,** 93–98.e1 CrossRef Medline
11. Nestler, A., Rylander, R., Kolisek, M., Nielsen, T., Ödman, N., Vormann, J., and Bullarbo, M. (2014) Blood pressure in pregnancy and magnesium sensitive genes. *Pregnancy Hypertens.* **4,** 41–45 CrossRef Medline
12. Hirschler, V., Gonzalez, C., Maccallini, G., Molinari, C., and Castano, L. (2017) Association between blood pressure and magnesium and uric acid levels in indigenous Argentinean children at high altitude. *Am. J. Hum. Biol.* **29,** CrossRef Medline
13. Posadas-Sánchez, R., Posadas-Romero, C., Cardoso-Saldaña, G., Vargas-Alarcón, G., Villarreal-Molina, M. T., Pérez-Hernández, N., Rodríguez-Pérez, J. M., Medina-Urrutia, A., Jorge-Galarza, E., Juárez-Rojas, J. G., and Torres-Tamayo, M. (2016) Serum magnesium is inversely associated with coronary artery calcification in the Genetics of Atherosclerotic Disease (GEA) study. *Nutr. J.* **15,** 22 Medline
14. Liao, F., Folsom, A. R., and Brancati, F. L. (1998) Is low magnesium concentration a risk factor for coronary heart disease? The Atherosclerosis Risk in Communities (ARIC) Study. *Am. Heart J.* **136,** 480–490 CrossRef Medline
15. Sarrafzadegan, N., Khosravi-Boroujeni, H., Lotfizadeh, M., Pourmogaddas, A., and Salehi-Abargouei, A. (2016) Magnesium status and the metabolic syndrome: a systematic review and meta-analysis. *Nutrition* **32,** 409–417 CrossRef Medline
16. Huerta, M. G., Roemmich, J. N., Kington, M. L., Bovbjerg, V. E., Weltman, A. L., Holmes, V. F., Patrie, J. T., Rogol, A. D., and Nadler, J. L. (2005) Magnesium deficiency is associated with insulin resistance in obese children. *Diabetes Care* **28,** 1175–1181 CrossRef Medline
17. Corica, F., Corsonello, A., Ientile, R., Cucinotta, D., Di Benedetto, A., Perticone, F., Dominguez, L. J., and Barbagallo, M. (2006) Serum ionized magnesium levels in relation to metabolic syndrome in type 2 diabetic patients. *J. Am. Coll. Nutr.* **25,** 210–215 CrossRef Medline
18. Lima Mde, L., Cruz, T., Rodrigues, L. E., Bomfim, O., Melo, J., Correia, R., Porto, M., Cedro, A., and Vicente, E. (2009) Serum and intracellular magnesium deficiency in patients with metabolic syndrome–evidences for its relation to insulin resistance. *Diabetes Res. Clin. Pract.* **83,** 257–262 CrossRef Medline
19. Tin, A., Grams, M. E., Maruthur, N. M., Astor, B. C., Couper, D., Mosley, T. H., Selvin, E., Coresh, J., and Kao, W. H. (2015) Results from the Atherosclerosis Risk in Communities study suggest that low serum magnesium is associated with incident kidney disease. *Kidney Int.* **87,** 820–827 CrossRef Medline
20. Rebholz, C. M., Tin, A., Liu, Y., Kuczmarski, M. F., Evans, M. K., Zonderman, A. B., and Crews, D. C. (2016) Dietary magnesium and kidney function decline: the Healthy Aging in Neighborhoods of Diversity across the Life Span Study. *Am. J. Nephrol.* **44,** 381–387 CrossRef Medline
21. Schmiedl, A., and Schwille, P. O. (2003) Is magnesium a marker of disordered mineral metabolism in males with idiopathic recurrent calcium urolithiasis? Observations focussing on fasting magnesiuria and magnesiemia, protein and other substances in urine and plasma. *Magnes. Res.* **16,** 192–205 Medline
22. Peters, K. E., Chubb, S. A., Davis, W. A., and Davis, T. M. (2013) The relationship between hypomagnesemia, metformin therapy and cardiovascular disease complicating type 2 diabetes: the Fremantle Diabetes Study. *PLoS One* **8,** e74355 CrossRef Medline
23. Del Gobbo, L. C., Song, Y., Poirier, P., Dewailly, E., Elin, R. J., and Egeland, G. M. (2012) Low serum magnesium concentrations are associated with a high prevalence of premature ventricular complexes in obese adults with type 2 diabetes. *Cardiovasc. Diabetol.* **11,** 23 CrossRef Medline
24. Dey, R., Rajappa, M., Parameswaran, S., and Revathy, G. (2015) Hypomagnesemia and atherogenic dyslipidemia in chronic kidney disease: surrogate markers for increased cardiovascular risk. *Clin. Exp. Nephrol.* **19,** 1054–1061 CrossRef Medline
25. Sakaguchi, Y., Fujii, N., Shoji, T., Hayashi, T., Rakugi, H., and Isaka, Y. (2014) Hypomagnesemia is a significant predictor of cardiovascular and non-cardiovascular mortality in patients undergoing hemodialysis. *Kidney Int.* **85,** 174–181 CrossRef Medline
26. de Baaij, J. H., Hoenderop, J. G., and Bindels, R. J. (2015) Magnesium in man: implications for health and disease. *Physiol. Rev.* **95,** 1–46 CrossRef Medline
27. Brunette, M. G., Vigneault, N., and Carriere, S. (1974) Micropuncture study of magnesium transport along the nephron in the young rat. *Am. J. Physiol.* **227,** 891–896 Medline

28. Voets, T., Nilius, B., Hoefs, S., van der Kemp, A. W., Droogmans, G., Bindels, R. J., and Hoenderop, J. G. (2004) TRPM6 forms the Mg^{2+} influx channel involved in intestinal and renal Mg^{2+} absorption. *J. Biol. Chem.* **279,** 19–25 CrossRef Medline
29. Schlingmann, K. P., Weber, S., Peters, M., Niemann Nejsum, L., Vitzthum, H., Klingel, K., Kratz, M., Haddad, E., Ristoff, E., Dinour, D., Syrrou, M., Nielsen, S., Sassen, M., Waldegger, S., Seyberth, H. W., and Konrad, M. (2002) Hypomagnesemia with secondary hypocalcemia is caused by mutations in TRPM6, a new member of the TRPM gene family. *Nat. Genet.* **31,** 166–170 CrossRef Medline
30. Walder, R. Y., Landau, D., Meyer, P., Shalev, H., Tsolia, M., Borochowitz, Z., Boettger, M. B., Beck, G. E., Englehardt, R. K., Carmi, R., and Sheffield, V. C. (2002) Mutation of TRPM6 causes familial hypomagnesemia with secondary hypocalcemia. *Nat. Genet.* **31,** 171–174 CrossRef Medline
31. Walder, R. Y., Yang, B., Stokes, J. B., Kirby, P. A., Cao, X., Shi, P., Searby, C. C., Husted, R. F., and Sheffield, V. C. (2009) Mice defective in Trpm6 show embryonic mortality and neural tube defects. *Hum. Mol. Genet.* **18,** 4367–4375 CrossRef Medline
32. Nair, A. V., Hocher, B., Verkaart, S., van Zeeland, F., Pfab, T., Slowinski, T., Chen, Y. P., Schlingmann, K. P., Schaller, A., Gallati, S., Bindels, R. J., Konrad, M., and Hoenderop, J. G. (2012) Loss of insulin-induced activation of TRPM6 magnesium channels results in impaired glucose tolerance during pregnancy. *Proc. Natl. Acad. Sci. U.S.A.* **109,** 11324–11329 CrossRef Medline
33. Thebault, S., Alexander, R. T., Tiel Groenestege, W. M., Hoenderop, J. G., and Bindels, R. J. (2009) EGF increases TRPM6 activity and surface expression. *J. Am. Soc. Nephrol.* **20,** 78–85 CrossRef Medline
34. Groenestege, W. M., Hoenderop, J. G., van den Heuvel, L., Knoers, N., and Bindels, R. J. (2006) The epithelial Mg^{2+} channel transient receptor potential melastatin 6 is regulated by dietary Mg^{2+} content and estrogens. *J. Am. Soc. Nephrol.* **17,** 1035–1043 CrossRef Medline
35. Cao, G., van der Wijst, J., van der Kemp, A., van Zeeland, F., Bindels, R. J., and Hoenderop, J. G. (2009) Regulation of the epithelial Mg^{2+} channel TRPM6 by estrogen and the associated repressor protein of estrogen receptor activity (REA). *J. Biol. Chem.* **284,** 14788–14795 CrossRef Medline
36. Cao, G., Thébault, S., van der Wijst, J., van der Kemp, A., Lasonder, E., Bindels, R. J., and Hoenderop, J. G. (2008) RACK1 inhibits TRPM6 activity via phosphorylation of the fused α-kinase domain. *Curr. Biol.* **18,** 168–176 CrossRef Medline
37. Groenestege, W. M., Thébault, S., van der Wijst, J., van den Berg, D., Janssen, R., Tejpar, S., van den Heuvel, L. P., van Cutsem, E., Hoenderop, J. G., Knoers, N. V., and Bindels, R. J. (2007) Impaired basolateral sorting of pro-EGF causes isolated recessive renal hypomagnesemia. *J. Clin. Invest.* **117,** 2260–2267 CrossRef Medline
38. Corre, T., Arjona, F. J., Hayward, C., Youhanna, S., de Baaij, J. H. F., Belge, H., Nagele, N., Debaix, H., Blanchard, M. G., Traglia, M., Harris, S. E., Ulivi, S., Rueedi, R., Lamparter, D., Mace, A., *et al.* (2017) Genome-wide meta-analysis unravels interactions between magnesium homeostasis and metabolic phenotypes. *J. Am. Soc. Nephrol.* **29,** 335–348 CrossRef Medline
39. de Baaij, J. H., Groot Koerkamp, M. J., Lavrijsen, M., van Zeeland, F., Meijer, H., Holstege, F. C., Bindels, R. J., and Hoenderop, J. G. (2013) Elucidation of the distal convoluted tubule transcriptome identifies new candidate genes involved in renal Mg^{2+} handling. *Am. J. Physiol. Renal Physiol.* **305,** F1563–F1573 CrossRef Medline
40. Kemter, E., Rathkolb, B., Rozman, J., Hans, W., Schrewe, A., Landbrecht, C., Klaften, M., Ivandic, B., Fuchs, H., Gailus-Durner, V., Klingenspor, M., de Angelis, M. H., Wolf, E., Wanke, R., and Aigner, B. (2009) Novel missense mutation of uromodulin in mice causes renal dysfunction with alterations in urea handling, energy, and bone metabolism. *Am. J. Physiol. Renal Physiol.* **297,** F1391–F1398 CrossRef Medline
41. Kemter, E., Prueckl, P., Sklenak, S., Rathkolb, B., Habermann, F. A., Hans, W., Gailus-Durner, V., Fuchs, H., Hrabě de Angelis, M., Wolf, E., Aigner, B., and Wanke, R. (2013) Type of uromodulin mutation and allelic status influence onset and severity of uromodulin-associated kidney disease in mice. *Hum. Mol. Genet.* **22,** 4148–4163 CrossRef Medline
42. Bates, J. M., Raffi, H. M., Prasadan, K., Mascarenhas, R., Laszik, Z., Maeda, N., Hultgren, S. J., and Kumar, S. (2004) Tamm-Horsfall protein knockout mice are more prone to urinary tract infection: rapid communication. *Kidney Int.* **65,** 791–797 CrossRef Medline
43. Mo, L., Liaw, L., Evan, A. P., Sommer, A. J., Lieske, J. C., and Wu, X. R. (2007) Renal calcinosis and stone formation in mice lacking osteopontin, Tamm-Horsfall protein, or both. *Am. J. Physiol. Renal Physiol.* **293,** F1935–F1943 CrossRef Medline
44. Trudu, M., Janas, S., Lanzani, C., Debaix, H., Schaeffer, C., Ikehata, M., Citterio, L., Demaretz, S., Trevisani, F., Ristagno, G., Glaudemans, B., Laghmani, K., Dell'Antonio, G., SKIPOGH team, Loffing, J., *et al.* (2013) Common noncoding UMOD gene variants induce salt-sensitive hypertension and kidney damage by increasing uromodulin expression. *Nat. Med.* **19,** 1655–1660 CrossRef Medline
45. Mutig, K., Kahl, T., Saritas, T., Godes, M., Persson, P., Bates, J., Raffi, H., Rampoldi, L., Uchida, S., Hille, C., Dosche, C., Kumar, S., Castañeda-Bueno, M., Gamba, G., and Bachmann, S. (2011) Activation of the bumetanide-sensitive Na^+,K^+,$2Cl^-$ cotransporter (NKCC2) is facilitated by Tamm-Horsfall protein in a chloride-sensitive manner. *J. Biol. Chem.* **286,** 30200–30210 CrossRef Medline
46. Liu, Y., Goldfarb, D., El-Achkar, T. M., Lieske, J. C., and Wu, X. R. (2018) Tamm-Horsfall protein/uromodulin deficiency elicits tubular compensatory responses leading to hypertension and hyperuricemia. *Am. J. Physiol. Renal Physiol.* **314,** F1062–F1076 CrossRef Medline
47. Rampoldi, L., Scolari, F., Amoroso, A., Ghiggeri, G., and Devuyst, O. (2011) The rediscovery of uromodulin (Tamm-Horsfall protein): from tubulointerstitial nephropathy to chronic kidney disease. *Kidney Int.* **80,** 338–347 CrossRef Medline
48. Hoenderop, J. G., and Bindels, R. J. (2008) Calciotropic and magnesiotropic TRP channels. *Physiology* **23,** 32–40 CrossRef Medline
49. van Angelen, A. A., Glaudemans, B., van der Kemp, A. W., Hoenderop, J. G., and Bindels, R. J. (2013) Cisplatin-induced injury of the renal distal convoluted tubule is associated with hypomagnesaemia in mice. *Nephrol. Dial. Transplant.* **28,** 879–889 CrossRef Medline
50. Devuyst, O., Olinger, E., and Rampoldi, L. (2017) Uromodulin: from physiology to rare and complex kidney disorders. *Nat. Rev. Nephrol.* **13,** 525–544 CrossRef Medline
51. Santambrogio, S., Cattaneo, A., Bernascone, I., Schwend, T., Jovine, L., Bachi, A., and Rampoldi, L. (2008) Urinary uromodulin carries an intact ZP domain generated by a conserved C-terminal proteolytic cleavage. *Biochem. Biophys. Res. Commun.* **370,** 410–413 CrossRef Medline
52. Wolf, M. T., Wu, X. R., and Huang, C. L. (2013) Uromodulin upregulates TRPV5 by impairing caveolin-mediated endocytosis. *Kidney Int.* **84,** 130–137 CrossRef Medline
53. Rampoldi, L., Caridi, G., Santon, D., Boaretto, F., Bernascone, I., Lamorte, G., Tardanico, R., Dagnino, M., Colussi, G., Scolari, F., Ghiggeri, G. M., Amoroso, A., and Casari, G. (2003) Allelism of MCKD, FJHN and GCKD caused by impairment of uromodulin export dynamics. *Hum. Mol. Genet.* **12,** 3369–3384 CrossRef Medline
54. Bachmann, S., Dawnay, A. B., Bouby, N., and Bankir, L. (1991) Tamm-Horsfall protein excretion during chronic alterations in urinary concentration and protein intake in the rat. *Ren. Physiol. Biochem.* **14,** 236–245 Medline
55. Goodall, A. A., and Marshall, R. D. (1980) Effects of freezing on the estimated amounts of Tamm–Horsfall glycoprotein in urine, as determined by radioimmunoassay. *Biochem. J.* **189,** 533–539 CrossRef Medline
56. Jovine, L., Qi, H., Williams, Z., Litscher, E., and Wassarman, P. M. (2002) The ZP domain is a conserved module for polymerization of extracellular proteins. *Nat. Cell Biol.* **4,** 457–461 CrossRef Medline
57. Lee, J. W., Chou, C. L., and Knepper, M. A. (2015) Deep sequencing in microdissected renal tubules identifies nephron segment-specific transcriptomes. *J. Am. Soc. Nephrol.* **26,** 2669–2677 CrossRef Medline
58. Kirchhausen, T., Macia, E., and Pelish, H. E. (2008) Use of dynasore, the small molecule inhibitor of dynamin, in the regulation of endocytosis. *Methods Enzymol.* **438,** 77–93 CrossRef Medline
59. Nie, M., Bal, M. S., Yang, Z., Liu, J., Rivera, C., Wenzel, A., Beck, B. B., Sakhaee, K., Marciano, D. K., and Wolf, M. T. (2016) Mucin-1 increases renal TRPV5 activity *in vitro*, and urinary level associates with calcium nephrolithiasis in patients. *J. Am. Soc. Nephrol.* **27,** 3447–3458 CrossRef Medline

60. Elola, M. T., Wolfenstein-Todel, C., Troncoso, M. F., Vasta, G. R., and Rabinovich, G. A. (2007) Galectins: matricellular glycan-binding proteins linking cell adhesion, migration, and survival. *Cell Mol. Life Sci.* **64,** 1679–1700 CrossRef Medline
61. Haudek, K. C., Patterson, R. J., and Wang, J. L. (2010) SR proteins and galectins: what's in a name? *Glycobiology* **20,** 1199–1207 CrossRef Medline
62. Demetriou, M., Granovsky, M., Quaggin, S., and Dennis, J. W. (2001) Negative regulation of T-cell activation and autoimmunity by Mgat5 *N*-glycosylation. *Nature* **409,** 733–739 CrossRef Medline
63. Cha, S. K., Ortega, B., Kurosu, H., Rosenblatt, K. P., Kuro-O, M., and Huang, C. L. (2008) Removal of sialic acid involving Klotho causes cell-surface retention of TRPV5 channel via binding to galectin-1. *Proc. Natl. Acad. Sci. U.S.A.* **105,** 9805–9810 CrossRef Medline
64. Wang, L., Li, F., Sun, W., Wu, S., Wang, X., Zhang, L., Zheng, D., Wang, J., and Gao, Y. (2006) Concanavalin A-captured glycoproteins in healthy human urine. *Mol. Cell. Proteomics* **5,** 560–562 CrossRef Medline
65. Ying, W. Z., and Sanders, P. W. (1998) Dietary salt regulates expression of Tamm-Horsfall glycoprotein in rats. *Kidney Int.* **54,** 1150–1156 CrossRef Medline
66. Torffvit, O., Melander, O., and Hultén, U. L. (2004) Urinary excretion rate of Tamm-Horsfall protein is related to salt intake in humans. *Nephron. Physiol.* **97,** 31–36 CrossRef Medline
67. Padmanabhan, S., Melander, O., Johnson, T., Di Blasio, A. M., Lee, W. K., Gentilini, D., Hastie, C. E., Menni, C., Monti, M. C., Delles, C., Laing, S., Corso, B., Navis, G., Kwakernaak, A. J., van der Harst, P., *et al.* (2010) Genome-wide association study of blood pressure extremes identifies variant near UMOD associated with hypertension. *PLoS Genet.* **6,** e1001177 CrossRef Medline
68. Schmitt, R., Kahl, T., Mutig, K., and Bachmann, S. (2004) Selectively reduced expression of thick ascending limb Tamm-Horsfall protein in hypothyroid kidneys. *Histochem. Cell Biol.* **121,** 319–327 CrossRef Medline
69. Bachmann, S., Mutig, K., Bates, J., Welker, P., Geist, B., Gross, V., Luft, F. C., Alenina, N., Bader, M., Thiele, B. J., Prasadan, K., Raffi, H. S., and Kumar, S. (2005) Renal effects of Tamm-Horsfall protein (uromodulin) deficiency in mice. *Am. J. Physiol. Renal Physiol.* **288,** F559–F567 CrossRef Medline
70. Renigunta, A., Renigunta, V., Saritas, T., Decher, N., Mutig, K., and Waldegger, S. (2011) Tamm-Horsfall glycoprotein interacts with renal outer medullary potassium channel ROMK2 and regulates its function. *J. Biol. Chem.* **286,** 2224–2235 CrossRef Medline
71. Liu, Y., Mo, L., Goldfarb, D. S., Evan, A. P., Liang, F., Khan, S. R., Lieske, J. C., and Wu, X. R. (2010) Progressive renal papillary calcification and ureteral stone formation in mice deficient for Tamm-Horsfall protein. *Am. J. Physiol. Renal Physiol.* **299,** F469–F478 CrossRef Medline
72. Tokonami, N., Takata, T., Beyeler, J., Ehrbar, I., Yoshifuji, A., Christensen, E. I., Loffing, J., Devuyst, O., and Olinger, E. G. (2018) Uromodulin is expressed in the distal convoluted tubule, where it is critical for regulation of the sodium chloride cotransporter NCC. *Kidney Int.* S0085-2538(18)30349-1 CrossRef Medline
73. Cha, S. K., Hu, M. C., Kurosu, H., Kuro-o, M., Moe, O., and Huang, C. L. (2009) Regulation of renal outer medullary potassium channel and renal K^+ excretion by Klotho. *Mol. Pharmacol.* **76,** 38–46 CrossRef Medline
74. Nio, J., Takahashi-Iwanaga, H., Morimatsu, M., Kon, Y., and Iwanaga, T. (2006) Immunohistochemical and *in situ* hybridization analysis of galectin-3, a β-galactoside binding lectin, in the urinary system of adult mice. *Histochem. Cell Biol.* **126,** 45–56 CrossRef Medline
75. Lech, M., Susanti, H. E., Römmele, C., Gröbmayr, R., Günthner, R., and Anders, H. J. (2012) Quantitative expression of C-type lectin receptors in humans and mice. *Int. J. Mol. Sci.* **13,** 10113–10131 CrossRef Medline
76. Picard, N., Van Abel, M., Campone, C., Seiler, M., Bloch-Faure, M., Hoenderop, J. G., Loffing, J., Meneton, P., Bindels, R. J., Paillard, M., Alhenc-Gelas, F., and Houillier, P. (2005) Tissue kallikrein-deficient mice display a defect in renal tubular calcium absorption. *J. Am. Soc. Nephrol.* **16,** 3602–3610 CrossRef Medline
77. Witkowski, M., Hubert, J., and Mazur, A. (2011) Methods of assessment of magnesium status in humans: a systematic review. *Magnes. Res.* **24,** 163–180 Medline
78. Arnaud, M. J. (2008) Update on the assessment of magnesium status. *Br. J. Nutr.* **99,** S24–S36 Medline
79. Elin, R. J. (2010) Assessment of magnesium status for diagnosis and therapy. *Magnes. Res.* **23,** S194–S198 Medline
80. Franz, K. B. (2004) A functional biological marker is needed for diagnosing magnesium deficiency. *J. Am. Coll. Nutr.* **23,** 738S–741S CrossRef Medline
81. Lameris, A. L., Hess, M. W., van Kruijsbergen, I., Hoenderop, J. G., and Bindels, R. J. (2013) Omeprazole enhances the colonic expression of the Mg^{2+} transporter TRPM6. *Pflugers Arch.* **465,** 1613–1620 CrossRef Medline
82. van Angelen, A. A., San-Cristobal, P., Pulskens, W. P., Hoenderop, J. G., and Bindels, R. J. (2013) The impact of dietary magnesium restriction on magnesiotropic and calciotropic genes. *Nephrol. Dial. Transplant.* **28,** 2983–2993 CrossRef Medline
83. Delgado, G. E., Kleber, M. E., Scharnagl, H., Krämer, B. K., März, W., and Scherberich, J. E. (2017) Serum uromodulin and mortality risk in patients undergoing coronary angiography. *J. Am. Soc. Nephrol.* **28,** 2201–2210 CrossRef Medline
84. Leiherer, A., Muendlein, A., Saely, C. H., Kinz, E., Brandtner, E. M., Fraunberger, P., and Drexel, H. (2017) Serum uromodulin is associated with impaired glucose metabolism. *Medicine* **96,** e5798 CrossRef Medline
85. Glauser, A., Hochreiter, W., Jaeger, P., and Hess, B. (2000) Determinants of urinary excretion of Tamm-Horsfall protein in non-selected kidney stone formers and healthy subjects. *Nephrol. Dial. Transplant.* **15,** 1580–1587 CrossRef Medline
86. Han, J., Liu, Y., Rao, F., Nievergelt, C. M., O'Connor, D. T., Wang, X., Liu, L., Bu, D., Liang, Y., Wang, F., Zhang, L., Zhang, H., Chen, Y., and Wang, H. (2013) Common genetic variants of the human uromodulin gene regulate transcription and predict plasma uric acid levels. *Kidney Int.* **83,** 733–740 CrossRef Medline
87. Köttgen, A., Hwang, S. J., Larson, M. G., Van Eyk, J. E., Fu, Q., Benjamin, E. J., Dehghan, A., Glazer, N. L., Kao, W. H., Harris, T. B., Gudnason, V., Shlipak, M. G., Yang, Q., Coresh, J., Levy, D., and Fox, C. S. (2010) Uromodulin levels associate with a common UMOD variant and risk for incident CKD. *J. Am. Soc. Nephrol.* **21,** 337–344 CrossRef Medline
88. Cha, S. K., Wu, T., and Huang, C. L. (2008) Protein kinase C inhibits caveolae-mediated endocytosis of TRPV5. *Am. J. Physiol. Renal Physiol.* **294,** F1212–F1221 CrossRef Medline
89. Hoorn, E. J., Walsh, S. B., McCormick, J. A., Fürstenberg, A., Yang, C. L., Roeschel, T., Paliege, A., Howie, A. J., Conley, J., Bachmann, S., Unwin, R. J., and Ellison, D. H. (2011) The calcineurin inhibitor tacrolimus activates the renal sodium chloride cotransporter to cause hypertension. *Nat. Med.* **17,** 1304–1309 CrossRef Medline
90. Lee, C. T., Chen, H. C., Lai, L. W., Yong, K. C., and Lien, Y. H. (2007) Effects of furosemide on renal calcium handling. *Am. J. Physiol. Renal Physiol.* **293,** F1231–F1237 CrossRef Medline